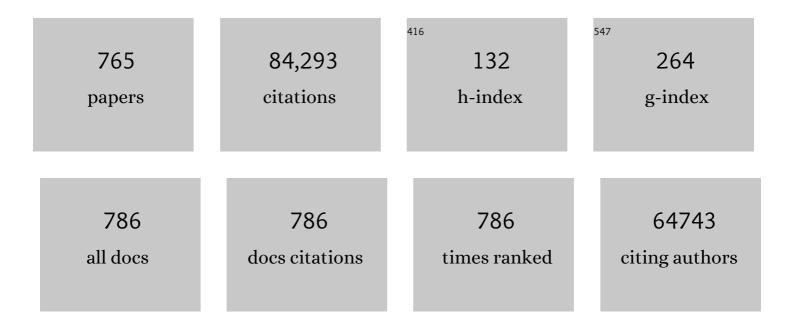
William Goddard

List of Publications by Year in descending order

Source: https://exaly.com/author-pdf/7227619/publications.pdf Version: 2024-02-01



#	Article	IF	CITATIONS
1	DREIDING: a generic force field for molecular simulations. The Journal of Physical Chemistry, 1990, 94, 8897-8909.	2.9	5,555
2	ReaxFF:Â A Reactive Force Field for Hydrocarbons. Journal of Physical Chemistry A, 2001, 105, 9396-9409.	1.1	4,490
3	Starburst Dendrimers: Molecular-Level Control of Size, Shape, Surface Chemistry, Topology, and Flexibility from Atoms to Macroscopic Matter. Angewandte Chemie International Edition in English, 1990, 29, 138-175.	4.4	3,032
4	Charge equilibration for molecular dynamics simulations. The Journal of Physical Chemistry, 1991, 95, 3358-3363.	2.9	2,910
5	Advances in molecular quantum chemistry contained in the Q-Chem 4 program package. Molecular Physics, 2015, 113, 184-215.	0.8	2,561
6	Silicon nanowires as efficient thermoelectric materials. Nature, 2008, 451, 168-171.	13.7	2,493
7	ReaxFF Reactive Force Field for Molecular Dynamics Simulations of Hydrocarbon Oxidation. Journal of Physical Chemistry A, 2008, 112, 1040-1053.	1.1	1,892
8	Ultrafine jagged platinum nanowires enable ultrahigh mass activity for the oxygen reduction reaction. Science, 2016, 354, 1414-1419.	6.0	1,292
9	Accurate First Principles Calculation of Molecular Charge Distributions and Solvation Energies from Ab Initio Quantum Mechanics and Continuum Dielectric Theory. Journal of the American Chemical Society, 1994, 116, 11875-11882.	6.6	1,026
10	ReaxFFSiO Reactive Force Field for Silicon and Silicon Oxide Systems. Journal of Physical Chemistry A, 2003, 107, 3803-3811.	1.1	821
11	High-performance bifunctional porous non-noble metal phosphide catalyst for overall water splitting. Nature Communications, 2018, 9, 2551.	5.8	812
12	Linear Artificial Molecular Muscles. Journal of the American Chemical Society, 2005, 127, 9745-9759.	6.6	660
13	Predictions of Hole Mobilities in Oligoacene Organic Semiconductors from Quantum Mechanical Calculationsâ€. Journal of Physical Chemistry B, 2004, 108, 8614-8621.	1.2	586
14	Calculation of Solvation Free Energies of Charged Solutes Using Mixed Cluster/Continuum Models. Journal of Physical Chemistry B, 2008, 112, 9709-9719.	1.2	567
15	Recent advances on simulation and theory of hydrogen storage in metal–organic frameworks and covalent organic frameworks. Chemical Society Reviews, 2009, 38, 1460.	18.7	535
16	Nonradiative Plasmon Decay and Hot Carrier Dynamics: Effects of Phonons, Surfaces, and Geometry. ACS Nano, 2016, 10, 957-966.	7.3	534
17	Software for the frontiers of quantum chemistry: An overview of developments in the Q-Chem 5 package. Journal of Chemical Physics, 2021, 155, 084801.	1.2	518
18	Shock Waves in High-Energy Materials: The Initial Chemical Events in Nitramine RDX. Physical Review Letters, 2003, 91, 098301.	2.9	495

#	Article	IF	CITATIONS
19	Sulfation patterns of glycosaminoglycans encode molecular recognition and activity. Nature Chemical Biology, 2006, 2, 467-473.	3.9	494
20	Oxidative Aliphatic C-H Fluorination with Fluoride Ion Catalyzed by a Manganese Porphyrin. Science, 2012, 337, 1322-1325.	6.0	478
21	Single-atom tailoring of platinum nanocatalysts for high-performance multifunctional electrocatalysis. Nature Catalysis, 2019, 2, 495-503.	16.1	464
22	Origin of low sodium capacity in graphite and generally weak substrate binding of Na and Mg among alkali and alkaline earth metals. Proceedings of the National Academy of Sciences of the United States of America, 2016, 113, 3735-3739.	3.3	462
23	Accurate Band Gaps for Semiconductors from Density Functional Theory. Journal of Physical Chemistry Letters, 2011, 2, 212-217.	2.1	444
24	Schottky-Barrier-Free Contacts with Two-Dimensional Semiconductors by Surface-Engineered MXenes. Journal of the American Chemical Society, 2016, 138, 15853-15856.	6.6	444
25	Mechanically bonded macromolecules. Chemical Society Reviews, 2010, 39, 17-29.	18.7	428
26	The two-phase model for calculating thermodynamic properties of liquids from molecular dynamics: Validation for the phase diagram of Lennard-Jones fluids. Journal of Chemical Physics, 2003, 119, 11792-11805.	1.2	426
27	Nanophase-Segregation and Transport in Nafion 117 from Molecular Dynamics Simulations:Â Effect of Monomeric Sequence. Journal of Physical Chemistry B, 2004, 108, 3149-3157.	1.2	425
28	Lithium-Doped Metal-Organic Frameworks for Reversible H2Storage at Ambient Temperature. Journal of the American Chemical Society, 2007, 129, 8422-8423.	6.6	418
29	Full atomistic reaction mechanism with kinetics for CO reduction on Cu(100) from ab initio molecular dynamics free-energy calculations at 298 K. Proceedings of the National Academy of Sciences of the United States of America, 2017, 114, 1795-1800.	3.3	414
30	Atomic level simulations on a million particles: The cell multipole method for Coulomb and London nonbond interactions. Journal of Chemical Physics, 1992, 97, 4309-4315.	1.2	404
31	ReaxFF- <i>l</i> g: Correction of the ReaxFF Reactive Force Field for London Dispersion, with Applications to the Equations of State for Energetic Materials. Journal of Physical Chemistry A, 2011, 115, 11016-11022.	1.1	401
32	Oxidation of Methanol on 2nd and 3rd Row Group VIII Transition Metals (Pt, Ir, Os, Pd, Rh, and Ru): Application to Direct Methanol Fuel Cells. Journal of the American Chemical Society, 1999, 121, 10928-10941.	6.6	397
33	Simulations on the Thermal Decomposition of a Poly(dimethylsiloxane) Polymer Using the ReaxFF Reactive Force Field. Journal of the American Chemical Society, 2005, 127, 7192-7202.	6.6	395
34	Oxygenâ€Vacancy Abundant Ultrafine Co ₃ O ₄ /Graphene Composites for Highâ€Rate Supercapacitor Electrodes. Advanced Science, 2018, 5, 1700659.	5.6	392
35	Development of the ReaxFF Reactive Force Field for Describing Transition Metal Catalyzed Reactions, with Application to the Initial Stages of the Catalytic Formation of Carbon Nanotubes. Journal of Physical Chemistry A, 2005, 109, 493-499.	1.1	390
36	Effect of Solvent and pH on the Structure of PAMAM Dendrimers. Macromolecules, 2005, 38, 979-991.	2.2	389

#	Article	IF	CITATIONS
37	Mechanistic Explanation of the pH Dependence and Onset Potentials for Hydrocarbon Products from Electrochemical Reduction of CO on Cu (111). Journal of the American Chemical Society, 2016, 138, 483-486.	6.6	381
38	Synergy between Fe and Ni in the optimal performance of (Ni,Fe)OOH catalysts for the oxygen evolution reaction. Proceedings of the National Academy of Sciences of the United States of America, 2018, 115, 5872-5877.	3.3	380
39	Selfâ€Consistent Procedures for Generalized Valence Bond Wavefunctions. Applications H3, BH, H2O, C2H6, and O2. Journal of Chemical Physics, 1972, 57, 738-748.	1.2	368
40	Thermal decomposition of RDX from reactive molecular dynamics. Journal of Chemical Physics, 2005, 122, 054502.	1.2	366
41	Subsurface oxide plays a critical role in CO ₂ activation by Cu(111) surfaces to form chemisorbed CO ₂ , the first step in reduction of CO ₂ . Proceedings of the National Academy of Sciences of the United States of America, 2017, 114, 6706-6711.	3.3	363
42	Melting and crystallization in Ni nanoclusters: The mesoscale regime. Journal of Chemical Physics, 2001, 115, 385-394.	1.2	345
43	Doubly hybrid density functional for accurate descriptions of nonbond interactions, thermochemistry, and thermochemical kinetics. Proceedings of the National Academy of Sciences of the United States of America, 2009, 106, 4963-4968.	3.3	332
44	Hildebrand and Hansen solubility parameters from Molecular Dynamics with applications to electronic nose polymer sensors. Journal of Computational Chemistry, 2004, 25, 1814-1826.	1.5	328
45	Evaluation of B3LYP, X3LYP, and M06-Class Density Functionals for Predicting the Binding Energies of Neutral, Protonated, and Deprotonated Water Clusters. Journal of Chemical Theory and Computation, 2009, 5, 1016-1026.	2.3	326
46	Monolayer atomic crystal molecular superlattices. Nature, 2018, 555, 231-236.	13.7	323
47	Cu metal embedded in oxidized matrix catalyst to promote CO ₂ activation and CO dimerization for electrochemical reduction of CO ₂ . Proceedings of the National Academy of Sciences of the United States of America, 2017, 114, 6685-6688.	3.3	322
48	Atomistic Mechanisms Underlying Selectivities in C ₁ and C ₂ Products from Electrochemical Reduction of CO on Cu(111). Journal of the American Chemical Society, 2017, 139, 130-136.	6.6	320
49	Prediction of fullerene packing in C60 and C70 crystals. Nature, 1991, 351, 464-467.	13.7	312
50	Efficient hydrogen evolution by ternary molybdenum sulfoselenide particles on self-standing porous nickel diselenide foam. Nature Communications, 2016, 7, 12765.	5.8	312
51	Reaction Mechanisms for the Electrochemical Reduction of CO ₂ to CO and Formate on the Cu(100) Surface at 298 K from Quantum Mechanics Free Energy Calculations with Explicit Water. Journal of the American Chemical Society, 2016, 138, 13802-13805.	6.6	310
52	Thermal conductivity of diamond and related materials from molecular dynamics simulations. Journal of Chemical Physics, 2000, 113, 6888-6900.	1.2	307
53	Unexpected discovery of low-cost maricite NaFePO ₄ as a high-performance electrode for Na-ion batteries. Energy and Environmental Science, 2015, 8, 540-545.	15.6	299
54	Highly active and stable stepped Cu surface for enhanced electrochemical CO2 reduction to C2H4. Nature Catalysis, 2020, 3, 804-812.	16.1	298

#	Article	IF	CITATIONS
55	Development and Validation of ReaxFF Reactive Force Field for Hydrocarbon Chemistry Catalyzed by Nickel. Journal of Physical Chemistry C, 2010, 114, 4939-4949.	1.5	288
56	Entropy and the driving force for the filling of carbon nanotubes with water. Proceedings of the National Academy of Sciences of the United States of America, 2011, 108, 11794-11798.	3.3	287
57	Radically enhanced molecular recognition. Nature Chemistry, 2010, 2, 42-49.	6.6	280
58	Theoretical studies of oxidative addition and reductive elimination. 3. Carbon-hydrogen and carbon-carbon reductive coupling from palladium and platinum bis(phosphine) complexes. Journal of the American Chemical Society, 1986, 108, 6115-6128.	6.6	279
59	Two-Phase Thermodynamic Model for Efficient and Accurate Absolute Entropy of Water from Molecular Dynamics Simulations. Journal of Physical Chemistry B, 2010, 114, 8191-8198.	1.2	277
60	In Silico Discovery of New Dopants for Fe-Doped Ni Oxyhydroxide (Ni _{1–<i>x</i>} Fe _{<i>x</i>} OOH) Catalysts for Oxygen Evolution Reaction. Journal of the American Chemical Society, 2018, 140, 6745-6748.	6.6	274
61	Mechanism of Câ^'F Reductive Elimination from Palladium(IV) Fluorides. Journal of the American Chemical Society, 2010, 132, 3793-3807.	6.6	273
62	Improved Quantum Theory of Many-Electron Systems. II. The Basic Method. Physical Review, 1967, 157, 81-93.	2.7	269
63	Strain Rate Induced Amorphization in Metallic Nanowires. Physical Review Letters, 1999, 82, 2900-2903.	2.9	268
64	Carbon Cluster Formation during Thermal Decomposition of Octahydro-1,3,5,7-tetranitro-1,3,5,7-tetrazocine and 1,3,5-Triamino-2,4,6-trinitrobenzene High Explosives from ReaxFF Reactive Molecular Dynamics Simulations. Journal of Physical Chemistry A, 2009, 113, 10619-10640.	1.1	257
65	Hydrogen bonding in the benzene–ammonia dimer. Nature, 1993, 362, 735-737.	13.7	254
66	Olefin metathesis - a mechanistic study of high-valent Group VI catalysts. Journal of the American Chemical Society, 1982, 104, 448-456.	6.6	251
67	PAMAM Dendrimers Undergo pH Responsive Conformational Changes without Swelling. Journal of the American Chemical Society, 2009, 131, 2798-2799.	6.6	249
68	Molecular Dynamics Study of a Surfactant-Mediated Decaneâ^'Water Interface:  Effect of Molecular Architecture of Alkyl Benzene Sulfonate. Journal of Physical Chemistry B, 2004, 108, 12130-12140.	1.2	244
69	The Reaction Mechanism with Free Energy Barriers at Constant Potentials for the Oxygen Evolution Reaction at the IrO ₂ (110) Surface. Journal of the American Chemical Society, 2017, 139, 149-155.	6.6	243
70	The Mechanism for Unimolecular Decomposition of RDX (1,3,5-Trinitro-1,3,5-triazine), an ab Initio Study. Journal of Physical Chemistry A, 2000, 104, 2261-2272.	1.1	241
71	ReaxFFMgHReactive Force Field for Magnesium Hydride Systems. Journal of Physical Chemistry A, 2005, 109, 851-859.	1.1	234
72	Explanation of Dramatic pH-Dependence of Hydrogen Binding on Noble Metal Electrode: Greatly Weakened Water Adsorption at High pH. Journal of the American Chemical Society, 2018, 140, 7787-7790.	6.6	234

#	Article	IF	CITATIONS
73	Selective Oxidation of Methane to Methanol Catalyzed, with Cï£;H Activation, by Homogeneous, Cationic Gold. Angewandte Chemie - International Edition, 2004, 43, 4626-4629.	7.2	229
74	Isolation of a Structural Mechanism for Uncoupling T Cell Receptor Signaling from Peptide-MHC Binding. Cell, 2018, 174, 672-687.e27.	13.5	229
75	Theoretical studies of oxidative addition and reductive elimination. 2. Reductive coupling of hydrogen-hydrogen, hydrogen-carbon, and carbon-carbon bonds from palladium and platinum complexes. Organometallics, 1986, 5, 609-622.	1.1	228
76	Force fields, structures, and properties of poly(vinylidene fluoride) crystals. Macromolecules, 1992, 25, 7268-7281.	2.2	227
77	Molecular dynamics study of the binaryCu46Zr54metallic glass motivated by experiments: Glass formation and atomic-level structure. Physical Review B, 2005, 71, .	1.1	227
78	Formation of carbon–nitrogen bonds in carbon monoxide electrolysis. Nature Chemistry, 2019, 11, 846-851.	6.6	223
79	Improved Quantum Theory of Many-Electron Systems. I. Construction of Eigenfunctions ofS^2Which Satisfy Pauli's Principle. Physical Review, 1967, 157, 73-80.	2.7	222
80	Configuration interaction studies of O3 and O+3. Ground and excited states. Journal of Chemical Physics, 1975, 62, 3912-3924.	1.2	221
81	Initiation Mechanisms and Kinetics of Pyrolysis and Combustion of JP-10 Hydrocarbon Jet Fuel. Journal of Physical Chemistry A, 2009, 113, 1740-1746.	1.1	213
82	Grand canonical electronic density-functional theory: Algorithms and applications to electrochemistry. Journal of Chemical Physics, 2017, 146, 114104.	1.2	211
83	Improved Quantum Theory of Manyâ€Electron Systems. V. The Spinâ€Coupling Optimized GI Method. Journal of Chemical Physics, 1969, 51, 1073-1087.	1.2	207
84	Free-Energy Barriers and Reaction Mechanisms for the Electrochemical Reduction of CO on the Cu(100) Surface, Including Multiple Layers of Explicit Solvent at pH 0. Journal of Physical Chemistry Letters, 2015, 6, 4767-4773.	2.1	206
85	An extended hybrid density functional (X3LYP) with improved descriptions of nonbond interactions and thermodynamic properties of molecular systems. Journal of Chemical Physics, 2005, 122, 014105.	1.2	204
86	Stabilizing Highly Active Ru Sites by Suppressing Lattice Oxygen Participation in Acidic Water Oxidation. Journal of the American Chemical Society, 2021, 143, 6482-6490.	6.6	204
87	The hindered rotor density-of-states interpolation function. Journal of Chemical Physics, 1997, 106, 6675-6680.	1.2	203
88	Resolution of the Band Gap Prediction Problem for Materials Design. Journal of Physical Chemistry Letters, 2016, 7, 1198-1203.	2.1	200
89	Poly(amidoamine) Dendrimers:  A New Class of High Capacity Chelating Agents for Cu(II) Ions. Environmental Science & Technology, 1999, 33, 820-824.	4.6	198
90	Theoretical Study of Solvent Effects on the Platinum-Catalyzed Oxygen Reduction Reaction. Journal of Physical Chemistry Letters, 2010, 1, 856-861.	2.1	195

#	Article	IF	CITATIONS
91	Embedding Covalency into Metal Catalysts for Efficient Electrochemical Conversion of CO ₂ . Journal of the American Chemical Society, 2014, 136, 11355-11361.	6.6	192
92	Engineering bacteria for production of rhamnolipid as an agent for enhanced oil recovery. Biotechnology and Bioengineering, 2007, 98, 842-853.	1.7	191
93	Ultrahigh Mass Activity for Carbon Dioxide Reduction Enabled by Gold–Iron Core–Shell Nanoparticles. Journal of the American Chemical Society, 2017, 139, 15608-15611.	6.6	191
94	Oxygen evolution reaction over catalytic single-site Co in a well-defined brookite TiO2 nanorod surface. Nature Catalysis, 2021, 4, 36-45.	16.1	189
95	Defect-enriched iron fluoride-oxide nanoporous thin films bifunctional catalyst for water splitting. Nature Communications, 2018, 9, 1809.	5.8	188
96	Mechanism of Homogeneous Ir(III) Catalyzed Regioselective Arylation of Olefins. Journal of the American Chemical Society, 2004, 126, 352-363.	6.6	184
97	Antiferromagnetic band structure ofLa2CuO4: Becke-3–Lee-Yang-Parr calculations. Physical Review B, 2001, 63, .	1.1	182
98	Design and study of homogeneous catalysts for the selective, low temperature oxidation of hydrocarbons. Journal of Molecular Catalysis A, 2006, 251, 8-23.	4.8	181
99	Electronic correlation and the Si(100) surface: Buckling versus nonbuckling. Journal of Vacuum Science and Technology, 1982, 21, 344-350.	1.9	180
100	Definitive Band Gaps for Single-Wall Carbon Nanotubes. Journal of Physical Chemistry Letters, 2010, 1, 2946-2950.	2.1	179
101	Contact Resistance for "End-Contacted―Metalâ^'Graphene and Metalâ^'Nanotube Interfaces from Quantum Mechanics. Journal of Physical Chemistry C, 2010, 114, 17845-17850.	1.5	177
102	Outstanding hydrogen evolution reaction catalyzed by porous nickel diselenide electrocatalysts. Energy and Environmental Science, 2017, 10, 1487-1492.	15.6	176
103	Alkylgold complexes by the intramolecular aminoauration of unactivated alkenes. Chemical Science, 2010, 1, 226.	3.7	174
104	Low-frequency and rare exome chip variants associate with fasting glucose and type 2 diabetes susceptibility. Nature Communications, 2015, 6, 5897.	5.8	173
105	The Reaction Mechanism with Free Energy Barriers for Electrochemical Dihydrogen Evolution on MoS ₂ . Journal of the American Chemical Society, 2015, 137, 6692-6698.	6.6	173
106	Effects of Surface Roughness on the Electrochemical Reduction of CO ₂ over Cu. ACS Energy Letters, 2020, 5, 1206-1214.	8.8	172
107	Highly stable tetrathiafulvalene radical dimers in [3]catenanes. Nature Chemistry, 2010, 2, 870-879.	6.6	171
108	Metalâ^'Organic Frameworks Provide Large Negative Thermal Expansion Behavior. Journal of Physical Chemistry C, 2007, 111, 15185-15191.	1.5	170

#	Article	IF	CITATIONS
109	Electrochemical CO Reduction Builds Solvent Water into Oxygenate Products. Journal of the American Chemical Society, 2018, 140, 9337-9340.	6.6	170
110	Dynamics of Lithium Dendrite Growth and Inhibition: Pulse Charging Experiments and Monte Carlo Calculations. Journal of Physical Chemistry Letters, 2014, 5, 1721-1726.	2.1	169
111	Mechanistic Study of Gold(I)-Catalyzed Intermolecular Hydroamination of Allenes. Journal of the American Chemical Society, 2010, 132, 13064-13071.	6.6	168
112	The charge-asymmetric nonlocally determined local-electric (CANDLE) solvation model. Journal of Chemical Physics, 2015, 142, 064107.	1.2	167
113	Efficient photocatalytic reduction of dinitrogen to ammonia on bismuth monoxide quantum dots. Journal of Materials Chemistry A, 2017, 5, 201-209.	5.2	160
114	BrÃ,nsted basicity of the air–water interface. Proceedings of the National Academy of Sciences of the United States of America, 2012, 109, 18679-18683.	3.3	159
115	A Radically Configurable Six-State Compound. Science, 2013, 339, 429-433.	6.0	158
116	Pressureâ€Dependent Polymorphism and Bandâ€Gap Tuning of Methylammonium Lead Iodide Perovskite. Angewandte Chemie - International Edition, 2016, 55, 6540-6544.	7.2	157
117	Development and Validation of a ReaxFF Reactive Force Field for Cu Cation/Water Interactions and Copper Metal/Metal Oxide/Metal Hydroxide Condensed Phases. Journal of Physical Chemistry A, 2010, 114, 9507-9514.	1.1	156
118	Mechanism for Unimolecular Decomposition of HMX (1,3,5,7-Tetranitro-1,3,5,7-tetrazocine), an ab Initio Study. Journal of Physical Chemistry A, 2001, 105, 1302-1314.	1.1	152
119	Non-conventional fluorescent biogenic and synthetic polymers without aromatic rings. Polymer Chemistry, 2017, 8, 1722-1727.	1.9	152
120	The extended Perdew-Burke-Ernzerhof functional with improved accuracy for thermodynamic and electronic properties of molecular systems. Journal of Chemical Physics, 2004, 121, 4068-4082.	1.2	150
121	Computational and experimental demonstrations of one-pot tandem catalysis for electrochemical carbon dioxide reduction to methane. Nature Communications, 2019, 10, 3340.	5.8	150
122	Atomic H-Induced Mo ₂ C Hybrid as an Active and Stable Bifunctional Electrocatalyst. ACS Nano, 2017, 11, 384-394.	7.3	149
123	Atomistic-Scale Simulations of the Initial Chemical Events in the Thermal Initiation of Triacetonetriperoxide. Journal of the American Chemical Society, 2005, 127, 11053-11062.	6.6	147
124	Mechanistic Analysis of Hydroarylation Catalysts. Journal of the American Chemical Society, 2004, 126, 11658-11665.	6.6	146
125	Nature of the Active Sites for CO Reduction on Copper Nanoparticles; Suggestions for Optimizing Performance. Journal of the American Chemical Society, 2017, 139, 11642-11645.	6.6	146
126	Correlationâ€consistent singlet–triplet gaps in substituted carbenes. Journal of Chemical Physics, 1988, 88, 1752-1763.	1.2	144

#	Article	IF	CITATIONS
127	Thermodynamics of liquids: standard molar entropies and heat capacities of common solvents from 2PT molecular dynamics. Physical Chemistry Chemical Physics, 2011, 13, 169-181.	1.3	144
128	A fast doubly hybrid density functional method close to chemical accuracy using a local opposite spin ansatz. Proceedings of the National Academy of Sciences of the United States of America, 2011, 108, 19896-19900.	3.3	143
129	Engineering the Composition and Crystallinity of Molybdenum Sulfide for High-Performance Electrocatalytic Hydrogen Evolution. ACS Catalysis, 2015, 5, 448-455.	5.5	141
130	Reaction mechanism and kinetics for CO2 reduction on nickel single atom catalysts from quantum mechanics. Nature Communications, 2020, 11, 2256.	5.8	140
131	Atomistic Explanation of Shear-Induced Amorphous Band Formation in Boron Carbide. Physical Review Letters, 2014, 113, 095501.	2.9	138
132	Mechanistic Analysis of Iridium Heteroatom Câ^'H Activation:  Evidence for an Internal Electrophilic Substitution Mechanism. Organometallics, 2007, 26, 1565-1567.	1.1	135
133	Ab InitioEffective Potentials for Use in Molecular Calculations. Journal of Chemical Physics, 1972, 56, 2685-2701.	1.2	134
134	Accurate Energies and Structures for Large Water Clusters Using the X3LYP Hybrid Density Functional. Journal of Physical Chemistry A, 2004, 108, 10518-10526.	1.1	134
135	A Highly Active Star Decahedron Cu Nanocatalyst for Hydrocarbon Production at Low Overpotentials. Advanced Materials, 2019, 31, e1805405.	11.1	134
136	Novel Family of Chiral-Based Topological Insulators: Elemental Tellurium under Strain. Physical Review Letters, 2013, 110, 176401.	2.9	133
137	Electrocatalysis at Organic–Metal Interfaces: Identification of Structure–Reactivity Relationships for CO ₂ Reduction at Modified Cu Surfaces. Journal of the American Chemical Society, 2019, 141, 7355-7364.	6.6	133
138	The Inner-Sphere Process in the Enantioselective Tsuji Allylation Reaction with (<i>S</i>)- <i>t</i> -Bu-phosphinooxazoline Ligands. Journal of the American Chemical Society, 2007, 129, 11876-11877.	6.6	129
139	Density-Dependent Liquid Nitromethane Decomposition: Molecular Dynamics Simulations Based on ReaxFF. Journal of Physical Chemistry A, 2011, 115, 10181-10202.	1.1	129
140	CH Activation with an O-Donor Iridiumâ^'Methoxo Complex. Journal of the American Chemical Society, 2005, 127, 14172-14173.	6.6	128
141	Mechanism for Degradation of Nafion in PEM Fuel Cells from Quantum Mechanics Calculations. Journal of the American Chemical Society, 2011, 133, 19857-19863.	6.6	128
142	Decomposition of Condensed Phase Energetic Materials: Interplay between Uni- and Bimolecular Mechanisms. Journal of the American Chemical Society, 2014, 136, 4192-4200.	6.6	126
143	Reaction Mechanism and Kinetics for Ammonia Synthesis on the Fe(111) Surface. Journal of the American Chemical Society, 2018, 140, 6288-6297.	6.6	126
144	Contact Resistance Properties between Nanotubes and Various Metals from Quantum Mechanics. Journal of Physical Chemistry C, 2007, 111, 11113-11116.	1.5	125

#	Article	IF	CITATIONS
145	Product Protection, the Key to Developing High Performance Methane Selective Oxidation Catalysts. Journal of the American Chemical Society, 2009, 131, 17110-17115.	6.6	124
146	Atomistic Description of Ionic Diffusion in PEO–LiTFSI: Effect of Temperature, Molecular Weight, and Ionic Concentration. Macromolecules, 2018, 51, 8987-8995.	2.2	124
147	Solution-Phase Mechanistic Study and Solid-State Structure of a Tris(bipyridinium radical cation) Inclusion Complex. Journal of the American Chemical Society, 2012, 134, 3061-3072.	6.6	123
148	The Hessian biased force field for silicon nitride ceramics: Predictions of thermodynamic and mechanical properties for α―and βâ€5i3N4. Journal of Chemical Physics, 1992, 97, 5048-5062.	1.2	122
149	Stability and Thermodynamics of the PtCl2Type Catalyst for Activating Methane to Methanol:Â A Computational Study. Organometallics, 2002, 21, 511-525.	1.1	121
150	Prediction of Vapor Pressures and Enthalpies of Vaporization Using a COSMO Solvation Model. Journal of Physical Chemistry A, 2004, 108, 7429-7439.	1.1	120
151	The ferroelectric and cubic phases in BaTiO3 ferroelectrics are also antiferroelectric. Proceedings of the United States of America, 2006, 103, 14695-14700.	3.3	119
152	Dynamics of the Dissociation of Hydrogen on Stepped Platinum Surfaces Using the ReaxFF Reactive Force Field. Journal of Physical Chemistry B, 2006, 110, 4274-4282.	1.2	116
153	Relevance of cis- and trans-dichloride Ru intermediates in Grubbs-II olefin metathesis catalysis (H2IMesCl2RuHR). Chemical Communications, 2008, , 6194.	2.2	116
154	Reaction Mechanism for the Hydrogen Evolution Reaction on the Basal Plane Sulfur Vacancy Site of MoS ₂ Using Grand Canonical Potential Kinetics. Journal of the American Chemical Society, 2018, 140, 16773-16782.	6.6	116
155	The 2s + 2s reactions at transition metals. 1. The reactions of deuterium with dichlorohydrotitanium(1+) ion (Cl2TiH+), titanium hydrogen dichloride (Cl2TiH), and scandium hydrogen dichloride (Cl2ScH). Journal of the American Chemical Society, 1984, 106, 308-311.	6.6	114
156	Fractal atomic-level percolation in metallic glasses. Science, 2015, 349, 1306-1310.	6.0	114
157	Proton–hydride tautomerism in hydrogen evolution catalysis. Proceedings of the National Academy of Sciences of the United States of America, 2016, 113, 6409-6414.	3.3	114
158	Relative Unidirectional Translation in an Artificial Molecular Assembly Fueled by Light. Journal of the American Chemical Society, 2013, 135, 18609-18620.	6.6	112
159	Polyyne Ring Nucleus Growth Model for Single-Layer Carbon Nanotubes. Physical Review Letters, 1996, 76, 2515-2518.	2.9	111
160	M3B:  A Coarse Grain Force Field for Molecular Simulations of Malto-Oligosaccharides and Their Water Mixtures. Journal of Physical Chemistry B, 2004, 108, 1414-1427.	1.2	111
161	A Push-Button Molecular Switch. Journal of the American Chemical Society, 2009, 131, 11571-11580.	6.6	111
162	Mechanism of metathesis and epoxidation in chromium and molybdenum complexes containing methyl-oxo bonds. Journal of the American Chemical Society, 1980, 102, 5114-5115.	6.6	110

#	Article	IF	CITATIONS
163	Computational Study of Copper(II) Complexation and Hydrolysis in Aqueous Solutions Using Mixed Cluster/Continuum Models. Journal of Physical Chemistry A, 2009, 113, 9559-9567.	1.1	110
164	Oxygen Hydration Mechanism for the Oxygen Reduction Reaction at Pt and Pd Fuel Cell Catalysts. Journal of Physical Chemistry Letters, 2011, 2, 572-576.	2.1	110
165	Atomistic Origin of Brittle Failure of Boron Carbide from Large-Scale Reactive Dynamics Simulations: Suggestions toward Improved Ductility. Physical Review Letters, 2015, 115, 105501.	2.9	109
166	Chemisorption of Atomic Oxygen on Pt(111) from DFT Studies of Pt-Clusters. Journal of Physical Chemistry B, 2003, 107, 9465-9476.	1.2	108
167	Water Formation on Pt and Pt-based Alloys: A Theoretical Description of a Catalytic Reaction. ChemPhysChem, 2006, 7, 992-1005.	1.0	107
168	General Multiobjective Force Field Optimization Framework, with Application to Reactive Force Fields for Silicon Carbide. Journal of Chemical Theory and Computation, 2014, 10, 1426-1439.	2.3	107
169	A rapid-response ultrasensitive biosensor for influenza virus detection using antibody modified boron-doped diamond. Scientific Reports, 2017, 7, 15707.	1.6	107
170	Identifying Active Sites for CO ₂ Reduction on Dealloyed Gold Surfaces by Combining Machine Learning with Multiscale Simulations. Journal of the American Chemical Society, 2019, 141, 11651-11657.	6.6	107
171	Using Photoelectron Spectroscopy and Quantum Mechanics to Determine d-Band Energies of Metals for Catalytic Applications. Journal of Physical Chemistry C, 2012, 116, 24016-24026.	1.5	106
172	Thermal Decomposition of Condensed-Phase Nitromethane from Molecular Dynamics from ReaxFF Reactive Dynamics. Journal of Physical Chemistry B, 2011, 115, 6534-6540.	1.2	105
173	Selective Extraction of C ₇₀ by a Tetragonal Prismatic Porphyrin Cage. Journal of the American Chemical Society, 2018, 140, 13835-13842.	6.6	105
174	Selective CO ₂ Electrochemical Reduction Enabled by a Tricomponent Copolymer Modifier on a Copper Surface. Journal of the American Chemical Society, 2021, 143, 2857-2865.	6.6	104
175	Thermal Decomposition of Hydrazines from Reactive Dynamics Using the ReaxFF Reactive Force Field. Journal of Physical Chemistry B, 2009, 113, 10770-10778.	1.2	103
176	Mechanism and Kinetics for the Initial Steps of Pyrolysis and Combustion of 1,6-Dicyclopropane-2,4-hexyne from ReaxFF Reactive Dynamics. Journal of Physical Chemistry A, 2011, 115, 4941-4950.	1.1	103
177	The Reaction Mechanism of the Enantioselective Tsuji Allylation: Inner-Sphere and Outer-Sphere Pathways, Internal Rearrangements, and Asymmetric C–C Bond Formation. Journal of the American Chemical Society, 2012, 134, 19050-19060.	6.6	103
178	Improved Quantum Theory of Manyâ€Electron Systems. III. The GF Method. Journal of Chemical Physics, 1968, 48, 450-461.	1.2	102
179	Oxygen induced promotion of electrochemical reduction of CO2 via co-electrolysis. Nature Communications, 2020, 11, 3844.	5.8	102
180	Initial Steps of Thermal Decomposition of Dihydroxylammonium 5,5′-bistetrazole-1,1′-diolate Crystals from Quantum Mechanics. Journal of Physical Chemistry C, 2014, 118, 27175-27181.	1.5	101

#	Article	IF	CITATIONS
181	Tellurium: Fast Electrical and Atomic Transport along the Weak Interaction Direction. Journal of the American Chemical Society, 2018, 140, 550-553.	6.6	101
182	Chemisorption of Organics on Platinum. 2. Chemisorption of C2Hxand CHxon Pt(111). Journal of Physical Chemistry B, 1998, 102, 9492-9500.	1.2	98
183	Development of the ReaxFF reactive force field for mechanistic studies of catalytic selective oxidation processes on BiMoO x. Topics in Catalysis, 2006, 38, 93.	1.3	98
184	Elucidating glycosaminoglycan–protein–protein interactions using carbohydrate microarray and computational approaches. Proceedings of the National Academy of Sciences of the United States of America, 2011, 108, 9747-9752.	3.3	98
185	Csp ³ –Csp ³ Bond-Forming Reductive Elimination from Well-Defined Copper(III) Complexes. Journal of the American Chemical Society, 2019, 141, 3153-3159.	6.6	98
186	Pd-Mediated Activation of Molecular Oxygen in a Nonpolar Medium. Journal of the American Chemical Society, 2005, 127, 13172-13179.	6.6	97
187	Physical mechanism of anisotropic sensitivity in pentaerythritol tetranitrate from compressive-shear reaction dynamics simulations. Applied Physics Letters, 2010, 96, .	1.5	97
188	Hydration of Copper(II): New Insights from Density Functional Theory and the COSMO Solvation Model. Journal of Physical Chemistry A, 2008, 112, 9104-9112.	1.1	96
189	Correlationâ€consistent configuration interaction: Accurate bond dissociation energies from simple wave functions. Journal of Chemical Physics, 1988, 88, 3132-3140.	1.2	95
190	A Covalent Organic Framework that Exceeds the DOE 2015 Volumetric Target for H ₂ Uptake at 298 K. Journal of Physical Chemistry Letters, 2012, 3, 2671-2675.	2.1	95
191	Oxygen Atom Transfer and Oxidative Water Incorporation in Cuboidal Mn ₃ MO _{<i>n</i>} Complexes Based on Synthetic, Isotopic Labeling, and Computational Studies. Journal of the American Chemical Society, 2013, 135, 1073-1082.	6.6	95
192	The gas phase reaction of singlet dioxygen with water: A water-catalyzed mechanism. Proceedings of the United States of America, 2002, 99, 3376-3381.	3.3	94
193	Two-Dimensional Halide Perovskites: Tuning Electronic Activities of Defects. Nano Letters, 2016, 16, 3335-3340.	4.5	94
194	Dynamics of Bengal Rose Encapsulated in the Meijer Dendrimer Box. Journal of the American Chemical Society, 1997, 119, 7458-7462.	6.6	93
195	Substrate Distortion to a Boat Conformation at Subsite â^1 Is Critical in the Mechanism of Family 18 Chitinases. Journal of the American Chemical Society, 1998, 120, 3571-3580.	6.6	93
196	Configuration interaction studies of the excited states of water. Journal of Chemical Physics, 1975, 62, 4325-4331.	1.2	92
197	Optimization and Application of Lithium Parameters for the Reactive Force Field, ReaxFF. Journal of Physical Chemistry A, 2005, 109, 4575-4582.	1.1	92
198	Ex2Box: Interdependent Modes of Binding in a Two-Nanometer-Long Synthetic Receptor. Journal of the American Chemical Society, 2013, 135, 12736-12746.	6.6	92

#	Article	IF	CITATIONS
199	Electronic Structure of IrO ₂ : The Role of the Metal d Orbitals. Journal of Physical Chemistry C, 2015, 119, 11570-11577.	1.5	91
200	Effectively Increased Efficiency for Electroreduction of Carbon Monoxide Using Supported Polycrystalline Copper Powder Electrocatalysts. ACS Catalysis, 2019, 9, 4709-4718.	5.5	91
201	Theoretical studies of Si and GaAs surfaces and initial steps in the oxidation. Journal of Vacuum Science and Technology, 1978, 15, 1274-1286.	1.9	90
202	Finding Correlations of the Oxygen Reduction Reaction Activity of Transition Metal Catalysts with Parameters Obtained from Quantum Mechanics. Journal of Physical Chemistry C, 2013, 117, 26598-26607.	1.5	89
203	The co-crystal of TNT/CL-20 leads to decreased sensitivity toward thermal decomposition from first principles based reactive molecular dynamics. Journal of Materials Chemistry A, 2015, 3, 5409-5419.	5.2	89
204	Protein simulations using techniques suitable for very large systems: The cell multipole method for nonbond interactions and the Newton-Euler inverse mass operator method for internal coordinate dynamics. Proteins: Structure, Function and Bioinformatics, 1994, 20, 227-247.	1.5	88
205	ReaxFF Reactive Force Field for Solid Oxide Fuel Cell Systems with Application to Oxygen Ion Transport in Yttria-Stabilized Zirconia. Journal of Physical Chemistry A, 2008, 112, 3133-3140.	1.1	88
206	Thermochemistry for Hydrocarbon Intermediates Chemisorbed on Metal Surfaces: CHn-m(CH3)m with n = 1, 2, 3 and m ≤n on Pt, Ir, Os, Pd, Rh, and Ru. Journal of the American Chemical Society, 2000, 122, 2309-2321.	6.6	87
207	Discrete Dimers of Redox-Active and Fluorescent Perylene Diimide-Based Rigid Isosceles Triangles in the Solid State. Journal of the American Chemical Society, 2019, 141, 1290-1303.	6.6	87
208	Anti-Markovnikov Hydroarylation of Unactivated Olefins Catalyzed by a Bis-tropolonato Iridium(III) Organometallic Complex. Organometallics, 2005, 24, 3229-3232.	1.1	86
209	Elucidation of the dynamics for hot-spot initiation at nonuniform interfaces of highly shocked materials. Physical Review B, 2011, 84, .	1.1	85
210	DFT Prediction of Oxygen Reduction Reaction on Palladium–Copper Alloy Surfaces. ACS Catalysis, 2014, 4, 1189-1197.	5.5	84
211	Highly Shocked Polymer Bonded Explosives at a Nonplanar Interface: Hot-Spot Formation Leading to Detonation. Journal of Physical Chemistry C, 2013, 117, 26551-26561.	1.5	83
212	Quantum Mechanics Reactive Dynamics Study of Solid Li-Electrode/Li ₆ PS ₅ Cl-Electrolyte Interface. ACS Energy Letters, 2017, 2, 1454-1459.	8.8	83
213	Bivalent spectator oxo bonds in metathesis and epoxidation alkenes. Nature, 1980, 285, 311-312.	13.7	82
214	Using Reduced Catalysts for Oxidation Reactions: Mechanistic Studies of the "Periana-Catalytica― System for CH ₄ Oxidation. Journal of the American Chemical Society, 2013, 135, 14644-14658.	6.6	82
215	Mechanism of Selective Oxidation and Ammoxidation of Propene on Bismuth Molybdates from DFT Calculations on Model Clusters. Journal of Physical Chemistry B, 2002, 106, 5997-6013.	1.2	81
216	Criteria for formation of metallic glasses: The role of atomic size ratio. Journal of Chemical Physics, 2003, 119, 9858-9870.	1.2	81

#	Article	IF	CITATIONS
217	Mechanism of Direct Molecular Oxygen Insertion in a Palladium(II)â^'Hydride Bond. Inorganic Chemistry, 2006, 45, 9631-9633.	1.9	81
218	The Critical Role of Phosphate in Vanadium Phosphate Oxide for the Catalytic Activation and Functionalization of <i>n</i> Butane to Maleic Anhydride. Journal of the American Chemical Society, 2013, 135, 4600-4603.	6.6	81
219	The Reaction Mechanism and Capacity Degradation Model in Lithium Insertion Organic Cathodes, Li ₂ C ₆ O ₆ , Using Combined Experimental and First Principle Studies. Journal of Physical Chemistry Letters, 2014, 5, 3086-3092.	2.1	81
220	Valenceâ€bond chargeâ€transfer solvation model for nonlinear optical properties of organic molecules in polar solvents. Journal of Chemical Physics, 1994, 101, 5860-5864.	1.2	79
221	Hydroxylation Structure and Proton Transfer Reactivity at the Zinc Oxideâ^'Water Interface. Journal of Physical Chemistry C, 2011, 115, 8573-8579.	1.5	79
222	Development of Interatomic ReaxFF Potentials for Au–S–C–H Systems. Journal of Physical Chemistry A, 2011, 115, 10315-10322.	1.1	77
223	Anisotropic shock sensitivity for <i>β</i> -octahydro-1,3,5,7-tetranitro-1,3,5,7-tetrazocine energetic material under compressive-shear loading from ReaxFF-lg reactive dynamics simulations. Journal of Applied Physics, 2012, 111, .	1.1	77
224	Conformational Analysis of Olefinâ^'Carbene Ruthenium Metathesis Catalysts. Organometallics, 2009, 28, 2643-2645.	1.1	76
225	Structure, Bonding, and Stability of a Catalytica Platinum(II) Catalyst:Â A Computational Study. Organometallics, 2003, 22, 2057-2068.	1.1	74
226	HierVLS Hierarchical Docking Protocol for Virtual Ligand Screening of Large-Molecule Databases. Journal of Medicinal Chemistry, 2004, 47, 56-71.	2.9	74
227	Single-Site Vanadyl Activation, Functionalization, and Reoxidation Reaction Mechanism for Propane Oxidative Dehydrogenation on the Cubic V4O10Cluster. Journal of Physical Chemistry C, 2007, 111, 5115-5127.	1.5	74
228	Chemisorption of H, Cl, Na, O, and S atoms on Ni(100) surfaces: A theoretical study using Ni20clusters. Critical Reviews in Solid State and Materials Sciences, 1981, 10, 261-296.	6.8	73
229	Mechanism and Energetics for Complexation of90Y with 1,4,7,10-Tetraazacyclododecane-1,4,7,10-tetraacetic Acid (DOTA), a Model for Cancer Radioimmunotherapy. Journal of the American Chemical Society, 1999, 121, 6142-6151.	6.6	73
230	Synthesis, Structure, and Reactivity of O-Donor Ir(III) Complexes:Â Câ^'H Activation Studies with Benzene. Journal of the American Chemical Society, 2005, 127, 11372-11389.	6.6	73
231	Identification of the Selective Sites for Electrochemical Reduction of CO to C ₂₊ Products on Copper Nanoparticles by Combining Reactive Force Fields, Density Functional Theory, and Machine Learning. ACS Energy Letters, 2018, 3, 2983-2988.	8.8	73
232	Grain Boundary Sliding and Amorphization are Responsible for the Reverse Hall-Petch Relation in Superhard Nanocrystalline Boron Carbide. Physical Review Letters, 2018, 121, 145504.	2.9	73
233	2s + 2s Reactions at transition metals. Part 3. Dichlorotitanacyclopropane. The structure and reactivity of a metallacyclopropane. Journal of the American Chemical Society, 1985, 107, 5027-5035.	6.6	72
234	Energetically Demanding Transport in a Supramolecular Assembly. Journal of the American Chemical Society, 2014, 136, 14702-14705.	6.6	72

#	Article	IF	CITATIONS
235	Structure-Based Sequence Alignment of the Transmembrane Domains of All Human GPCRs: Phylogenetic, Structural and Functional Implications. PLoS Computational Biology, 2016, 12, e1004805.	1.5	72
236	Ab Initio Calculations on the H2+D2=2HD Four enter Exchange Reaction. I. Elements of the Reaction Surface. Journal of Chemical Physics, 1969, 51, 716-731.	1.2	71
237	Hessianâ€biased force fields from combining theory and experiment. Journal of Chemical Physics, 1989, 90, 7207-7215.	1.2	71
238	Constant Temperature Constrained Molecular Dynamics:  The Newtonâ^'Euler Inverse Mass Operator Method. The Journal of Physical Chemistry, 1996, 100, 10508-10517.	2.9	70
239	Chemisorption of Organics on Platinum. 1. The Interstitial Electron Model. Journal of Physical Chemistry B, 1998, 102, 9481-9491.	1.2	70
240	Mechanism for antibody catalysis of the oxidation of water by singlet dioxygen. Proceedings of the National Academy of Sciences of the United States of America, 2002, 99, 2636-2641.	3.3	70
241	DFT Study of Oxygen Reduction Reaction on Os/Pt Core–Shell Catalysts Validated by Electrochemical Experiment. ACS Catalysis, 2015, 5, 1568-1580.	5.5	70
242	Energetics and Solvation Effects at the Photoanode/Catalyst Interface: Ohmic Contact versus Schottky Barrier. Journal of the American Chemical Society, 2015, 137, 5264-5267.	6.6	70
243	Reaction intermediates during operando electrocatalysis identified from full solvent quantum mechanics molecular dynamics. Proceedings of the National Academy of Sciences of the United States of America, 2019, 116, 7718-7722.	3.3	70
244	C–H activation in strongly acidic media. The co-catalytic effect of the reaction medium. Chemical Communications, 2009, , 2373.	2.2	69
245	3D Structure Prediction of TAS2R38 Bitter Receptors Bound to Agonists Phenylthiocarbamide (PTC) and 6-n-Propylthiouracil (PROP). Journal of Chemical Information and Modeling, 2012, 52, 1875-1885.	2.5	69
246	Anisotropic Shock Sensitivity of Cyclotrimethylene Trinitramine (RDX) from Compress-and-Shear Reactive Dynamics. Journal of Physical Chemistry C, 2012, 116, 10198-10206.	1.5	69
247	<scp>G</scp> proteinâ€coupled odorant receptors: From sequence to structure. Protein Science, 2015, 24, 1543-1548.	3.1	69
248	In Silico Design of Highly Selective Mo-V-Te-Nb-O Mixed Metal Oxide Catalysts for Ammoxidation and Oxidative Dehydrogenation of Propane and Ethane. Journal of the American Chemical Society, 2015, 137, 13224-13227.	6.6	68
249	A Mn Bipyrimidine Catalyst Predicted To Reduce CO ₂ at Lower Overpotential. ACS Catalysis, 2015, 5, 2521-2528.	5.5	67
250	Thermal relaxation of lithium dendrites. Physical Chemistry Chemical Physics, 2015, 17, 8000-8005.	1.3	66
251	A candidate LiBH4 for hydrogen storage: Crystal structures and reaction mechanisms of intermediate phases. Applied Physics Letters, 2005, 87, 111904.	1.5	65
252	Compressive Shear Reactive Molecular Dynamics Studies Indicating That Cocrystals of TNT/CL-20 Decrease Sensitivity. Journal of Physical Chemistry C, 2014, 118, 30202-30208.	1.5	65

#	Article	IF	CITATIONS
253	Folding of Oligoviologens Induced by Radical–Radical Interactions. Journal of the American Chemical Society, 2015, 137, 876-885.	6.6	65
254	Antifreeze proteins govern the precipitation of trehalose in a freezing-avoiding insect at low temperature. Proceedings of the National Academy of Sciences of the United States of America, 2016, 113, 6683-6688.	3.3	65
255	Activation mechanism of the G protein-coupled sweet receptor heterodimer with sweeteners and allosteric agonists. Proceedings of the National Academy of Sciences of the United States of America, 2017, 114, 2568-2573.	3.3	65
256	Wavefunctions and Correlation Energies for Twoâ€, Threeâ€, and Fourâ€Electron Atoms. Journal of Chemical Physics, 1968, 48, 1008-1017.	1.2	64
257	How broadly tuned olfactory receptors equally recognize their agonists. Human OR1G1 as a test case. Cellular and Molecular Life Sciences, 2012, 69, 4205-4213.	2.4	64
258	First-Principles-Based Reaction Kinetics for Decomposition of Hot, Dense Liquid TNT from ReaxFF Multiscale Reactive Dynamics Simulations. Journal of Physical Chemistry C, 2013, 117, 21043-21054.	1.5	64
259	Au-activated N motifs in non-coherent cupric porphyrin metal organic frameworks for promoting and stabilizing ethylene production. Nature Communications, 2022, 13, 63.	5.8	64
260	Configuration interaction studies on lowâ€lying states of O2. Journal of Chemical Physics, 1975, 63, 3523-3531.	1.2	63
261	Selective oxidation and ammoxidation of propene on bismuth molybdates, ab initio calculations. Topics in Catalysis, 2001, 15, 273-289.	1.3	63
262	Dramatic differences in carbon dioxide adsorption and initial steps of reduction between silver and copper. Nature Communications, 2019, 10, 1875.	5.8	63
263	Doubleâ€Exchangeâ€Induced in situ Conductivity in Nickelâ€Based Oxyhydroxides: An Effective Descriptor for Electrocatalytic Oxygen Evolution. Angewandte Chemie - International Edition, 2021, 60, 16448-16456.	7.2	63
264	Reconstruction and oxidation of the GaAs(110) surface. Journal of Vacuum Science and Technology, 1979, 16, 1178-1185.	1.9	62
265	Mechanism for Oxygen Reduction Reaction on Pt ₃ Ni Alloy Fuel Cell Cathode. Journal of Physical Chemistry C, 2012, 116, 21334-21342.	1.5	62
266	Superstrength through Nanotwinning. Nano Letters, 2016, 16, 7573-7579.	4.5	62
267	Molecular Russian dolls. Nature Communications, 2018, 9, 5275.	5.8	61
268	Surface Ligand Promotion of Carbon Dioxide Reduction through Stabilizing Chemisorbed Reactive Intermediates. Journal of Physical Chemistry Letters, 2018, 9, 3057-3061.	2.1	61
269	Theoretical studies of the reconstruction of the (110) surface of Ill–V and Il–VI semiconductor compounds. Journal of Vacuum Science and Technology, 1980, 17, 982-986.	1.9	60
270	First-principles approach to the charge-transport characteristics of monolayer molecular-electronics devices: Application to hexanedithiolate devices. Physical Review B, 2006, 73, .	1.1	60

#	Article	IF	CITATIONS
271	Transition State Energy Decomposition Study of Acetate-Assisted and Internal Electrophilic Substitution Câ^'H Bond Activation by (acac-O,O) ₂ Ir(X) Complexes (X =) Tj ETQq1 1 0.784314 rgBT	/Qvzerlock	160Tf 50 73
272	Transition-State Charge Transfer Reveals Electrophilic, Ambiphilic, and Nucleophilic Carbonâ^'Hydrogen Bond Activation. Journal of the American Chemical Society, 2009, 131, 11686-11688.	6.6	60
273	Brittle Failure Mechanism in Thermoelectric Skutterudite CoSb ₃ . Chemistry of Materials, 2015, 27, 6329-6336.	3.2	60
274	Use of Ab Initio G1 Effective Potentials for Calculations of Molecular Excited States. Journal of Chemical Physics, 1972, 56, 3342-3348.	1.2	59
275	The ReaxFF Monte Carlo Reactive Dynamics Method for Predicting Atomistic Structures of Disordered Ceramics: Application to the Mo ₃ VO _{<i>x</i>} Catalyst. Angewandte Chemie - International Edition, 2009, 48, 7630-7634.	7.2	59
276	Pb-Activated Amine-Assisted Photocatalytic Hydrogen Evolution Reaction on Organic–Inorganic Perovskites. Journal of the American Chemical Society, 2018, 140, 1994-1997.	6.6	59
277	Density functional theory based neural network force fields from energy decompositions. Physical Review B, 2019, 99, .	1.1	59
278	Methane Activation by Transition-Metal Oxides, MOx(M = Cr, Mo, W;x= 1, 2, 3). Journal of Physical Chemistry A, 2002, 106, 7171-7176.	1.1	58
279	Cyclooctyne-based reagents for uncatalyzed click chemistry: A computational survey. Organic and Biomolecular Chemistry, 2009, 7, 5255.	1.5	58
280	Predicted 3D structures for adenosine receptors bound to ligands: Comparison to the crystal structure. Journal of Structural Biology, 2010, 170, 10-20.	1.3	58
281	Predicted Optimal Bifunctional Electrocatalysts for the Hydrogen Evolution Reaction and the Oxygen Evolution Reaction Using Chalcogenide Heterostructures Based on Machine Learning Analysis of in Silico Quantum Mechanics Based High Throughput Screening. Journal of Physical Chemistry Letters, 2020, 11, 869-876.	2.1	58
282	Zeolitic Imidazolate Frameworks as H2 Adsorbents: Ab Initio Based Grand Canonical Monte Carlo Simulation. Journal of Physical Chemistry C, 2010, 114, 12039-12047.	1.5	57
283	Experimental Sabatier plot for predictive design of active and stable Pt-alloy oxygen reduction reaction catalysts. Nature Catalysis, 2022, 5, 513-523.	16.1	57
284	Nonlinear partial differential equations and applications: Peroxone chemistry: Formation of H2O3 and ring-(HO2)(HO3) from O3/H2O2. Proceedings of the National Academy of Sciences of the United States of America, 2002, 99, 15308-15312.	3.3	56
285	Structures, Mechanisms, and Kinetics of Selective Ammoxidation and Oxidation of Propane over Multi-metal Oxide Catalysts. Topics in Catalysis, 2008, 50, 2-18.	1.3	56
286	Atomic-Level Understanding of "Asymmetric Twins―in Boron Carbide. Physical Review Letters, 2015, 115, 175501.	2.9	56
287	The role of kinetic energy in chemical binding. Theoretica Chimica Acta, 1972, 26, 211-230.	0.9	55
288	Anions dramatically enhance proton transfer through aqueous interfaces. Proceedings of the	3.3	55

National Academy of Sciences of the United States of America, 2012, 109, 10228-10232.

#	Article	IF	CITATIONS
289	Redox Control of the Binding Modes of an Organic Receptor. Journal of the American Chemical Society, 2015, 137, 11057-11068.	6.6	55
290	Atomistic Explanation of the Dramatically Improved Oxygen Reduction Reaction of Jagged Platinum Nanowires, 50 Times Better than Pt. Journal of the American Chemical Society, 2020, 142, 8625-8632.	6.6	55
291	The theoretical study on interaction of hydrogen with single-walled boron nitride nanotubes. I. The reactive force field ReaxFFHBN development. Journal of Chemical Physics, 2005, 123, 114703.	1.2	54
292	Structures, Energetics, and Reaction Barriers for CHx Bound to the Nickel (111) Surface. Journal of Physical Chemistry C, 2009, 113, 20290-20306.	1.5	54
293	Proton or Metal? The H/D Exchange of Arenes in Acidic Solvents. ACS Catalysis, 2015, 5, 769-775.	5.5	54
294	Ductile deformation mechanism in semiconductor $\hat{l}\pm$ -Ag2S. Npj Computational Materials, 2018, 4, .	3.5	54
295	Generalized extended empirical bond-order dependent force fields including nonbond interactions. Theoretical Chemistry Accounts, 1999, 102, 346-354.	0.5	53
296	Prediction of the 3D Structure and Dynamics of Human DP C-Protein Coupled Receptor Bound to an Agonist and an Antagonist. Journal of the American Chemical Society, 2007, 129, 10720-10731.	6.6	53
297	Donor–Acceptor Oligorotaxanes Made to Order. Chemistry - A European Journal, 2011, 17, 2107-2119.	1.7	53
298	Adaptive Accelerated ReaxFF Reactive Dynamics with Validation from Simulating Hydrogen Combustion. Journal of the American Chemical Society, 2014, 136, 9434-9442.	6.6	53
299	The atomistic origin of the extraordinary oxygen reduction activity of Pt ₃ Ni ₇ fuel cell catalysts. Chemical Science, 2015, 6, 3915-3925.	3.7	53
300	Superstrengthening <mml:math <br="" xmlns:mml="http://www.w3.org/1998/Math/MathML">display="inline"><mml:mrow><mml:msub><mml:mrow><mml:mi>Bi</mml:mi></mml:mrow><mml:mn>2through Nanotwinning. Physical Review Letters, 2017, 119, 085501.</mml:mn></mml:msub></mml:mrow></mml:math>	:m 2 39(mr	nl:m s ub> <mm< td=""></mm<>
301	The importance of grand-canonical quantum mechanical methods to describe the effect of electrode potential on the stability of intermediates involved in both electrochemical CO ₂ reduction and hydrogen evolution. Physical Chemistry Chemical Physics, 2018, 20, 2549-2557.	1.3	53
302	Electronic Structure of LiH According to a Generalization of the Valenceâ€Bond Method. Journal of Chemical Physics, 1969, 50, 4524-4532.	1.2	52
303	Alkali oxide diatomics: Explanation of the change in ground state symmetry from LiO(2Î) CsO(2Σ+). Journal of Chemical Physics, 1982, 77, 4259-4261.	1.2	52
304	Electron correlation, basis sets, and the methylene singlet–triplet gap. Journal of Chemical Physics, 1987, 86, 862-865.	1.2	52
305	Nanofiltration membranes based on polyvinylidene fluoride nanofibrous scaffolds and crosslinked polyethyleneimine networks. Journal of Nanoparticle Research, 2012, 14, 1.	0.8	52
306	Probing the C–O Bond-Formation Step in Metalloporphyrin-Catalyzed C–H Oxygenation Reactions. ACS Catalysis, 2017, 7, 4182-4188.	5.5	52

#	Article	IF	CITATIONS
307	Characterization of Nanoparticles and Colloids in Aquatic Systems 1. Small Angle Neutron Scattering Investigations of Suwannee River Fulvic Acid Aggregates in Aqueous Solutions. Journal of Nanoparticle Research, 2005, 7, 435-448.	0.8	51
308	Mechanism of Selective Oxidation of Propene to Acrolein on Bismuth Molybdates from Quantum Mechanical Calculations. Journal of Physical Chemistry C, 2007, 111, 16405-16415.	1.5	51
309	Predicted structure of agonist-bound glucagon-like peptide 1 receptor, a class B G protein-coupled receptor. Proceedings of the National Academy of Sciences of the United States of America, 2012, 109, 19988-19993.	3.3	51
310	Design of a Graphene Nitrene Two-Dimensional Catalyst Heterostructure Providing a Well-Defined Site Accommodating One to Three Metals, with Application to CO ₂ Reduction Electrocatalysis for the Two-Metal Case. Journal of Physical Chemistry Letters, 2020, 11, 2541-2549.	2.1	51
311	Electron-catalysed molecular recognition. Nature, 2022, 603, 265-270.	13.7	51
312	Pd-Mediated Activation of Molecular Oxygen:Â Pd(0) versus Direct Insertion. Journal of the American Chemical Society, 2007, 129, 10361-10369.	6.6	50
313	Ideal Strength and Deformation Mechanism in High-Efficiency Thermoelectric SnSe. Chemistry of Materials, 2017, 29, 2382-2389.	3.2	50
314	Compressed Intermetallic PdCu for Enhanced Electrocatalysis. ACS Energy Letters, 2020, 5, 3672-3680.	8.8	50
315	The generalized valence bond description of O2. Journal of Chemical Physics, 1975, 63, 4632-4639.	1.2	49
316	Study of surfaces and interfaces using quantum chemistry techniques. Journal of Vacuum Science and Technology, 1979, 16, 1308-1317.	1.9	49
317	Theoretical studies of electron transfer in metal dimers: XY+→X+Y, where X, Y=Be, Mg, Ca, Zn, Cd. Journal of Chemical Physics, 1987, 87, 926-935.	1.2	49
318	GVB-RP: A reliable MCSCF wave function for large systems. International Journal of Quantum Chemistry, 1999, 73, 1-22.	1.0	49
319	Interfacial Reactions of Ozone with Surfactant Protein B in a Model Lung Surfactant System. Journal of the American Chemical Society, 2010, 132, 2254-2263.	6.6	49
320	Gas-Phase Lubrication of ta-C by Glycerol and Hydrogen Peroxide. Experimental and Computer Modeling. Journal of Physical Chemistry C, 2010, 114, 5003-5011.	1.5	49
321	Enhanced ideal strength of thermoelectric half-Heusler TiNiSn by sub-structure engineering. Journal of Materials Chemistry A, 2016, 4, 14625-14636.	5.2	48
322	Direct comparisons of rates for low temperature diffusion of hydrogen and deuterium on Cu(001) from quantum mechanical calculations and scanning tunneling microscopy experiments. Journal of Chemical Physics, 2001, 115, 5620-5624.	1.2	47
323	Hydrogen storage in LiAlH4: Predictions of the crystal structures and reaction mechanisms of intermediate phases from quantum mechanics. Journal of Chemical Physics, 2004, 121, 10623-10633.	1.2	47
324	Predictions of melting, crystallization, and local atomic arrangements of aluminum clusters using a reactive force field. Journal of Chemical Physics, 2008, 129, 244506.	1.2	47

#	Article	IF	CITATIONS
325	Chemistries for Patterning Robust DNA MicroBarcodes Enable Multiplex Assays of Cytoplasm Proteins from Single Cancer Cells. ChemPhysChem, 2010, 11, 3063-3069.	1.0	47

$_{326}$ Universal Correction of Density Functional Theory to Include London Dispersion (up to Lr, Element) Tj ETQq0 0 0 rgBT /Overlock 10 Tf 50 $_{2.1}^{+0.00}$

327	Mechanical Bonds and Topological Effects in Radical Dimer Stabilization. Journal of the American Chemical Society, 2014, 136, 11011-11026.	6.6	47
328	Solvation effects on the band edge positions of photocatalysts from first principles. Physical Chemistry Chemical Physics, 2015, 17, 30499-30509.	1.3	47
329	Oligorotaxane Radicals under Orders. ACS Central Science, 2016, 2, 89-98.	5.3	47
330	Structure of polyamidoamide dendrimers up to limiting generations: A mesoscale description. Journal of Chemical Physics, 2009, 130, 144902.	1.2	46
331	Microalloying Boron Carbide with Silicon to Achieve Dramatically Improved Ductility. Journal of Physical Chemistry Letters, 2014, 5, 4169-4174.	2.1	46
332	Role of solvent-anion charge transfer in oxidative degradation of battery electrolytes. Nature Communications, 2019, 10, 3360.	5.8	46
333	Improved Quantum Theory of Manyâ€Electron Systems. IV. Properties of GF Wavefunctions. Journal of Chemical Physics, 1968, 48, 5337-5347.	1.2	45
334	Chemisorption of Al and Ga on the GaAs (110) surface. Journal of Vacuum Science and Technology, 1980, 17, 869-873.	1.9	45
335	Charge density waves, spin density waves, and Peierls distortions in oneâ€dimensional metals. I. Hartree–Fock studies of Cu, Ag, Au, Li, and Na. Journal of Chemical Physics, 1988, 88, 277-302.	1.2	45
336	A theoretical study of the conversion of gas phase methanediol to formaldehyde. Journal of Chemical Physics, 2003, 119, 5117-5120.	1.2	45
337	Charge and polarization distributions at the 90° domain wall in barium titanate ferroelectric. Applied Physics Letters, 2006, 89, 182903.	1.5	45
338	Flat-Bottom Strategy for Improved Accuracy in Protein Side-Chain Placements. Journal of Chemical Theory and Computation, 2008, 4, 2160-2169.	2.3	45
339	Explanation of the Colossal Detonation Sensitivity of Silicon Pentaerythritol Tetranitrate (Si-PETN) Explosive. Journal of the American Chemical Society, 2009, 131, 7490-7491.	6.6	45
340	Micro- and Macromechanical Properties of Thermoelectric Lead Chalcogenides. ACS Applied Materials & Interfaces, 2017, 9, 40488-40496.	4.0	45
341	Singlet–triplet energy gaps in fluorineâ€substituted methylenes and silylenes. Journal of Chemical Physics, 1990, 93, 4986-4993.	1.2	44
342	Effect of cyclic chain architecture on properties of dilute solutions of polyethylene from molecular dynamics simulations. Journal of Chemical Physics, 2003, 119, 1843-1854.	1.2	44

#	Article	IF	CITATIONS
343	Theoretical study on interaction of hydrogen with single-walled boron nitride nanotubes. II. Collision, storage, and adsorption. Journal of Chemical Physics, 2005, 123, 114704.	1.2	44
344	Absolute Entropy and Energy of Carbon Dioxide Using the Two-Phase Thermodynamic Model. Journal of Chemical Theory and Computation, 2011, 7, 1893-1901.	2.3	44
345	Bihelix: Towards <i>de novo</i> structure prediction of an ensemble of Gâ€protein coupled receptor conformations. Proteins: Structure, Function and Bioinformatics, 2012, 80, 505-518.	1.5	44
346	New Ground-State Crystal Structure of Elemental Boron. Physical Review Letters, 2016, 117, 085501.	2.9	44
347	Test of the Binding Threshold Hypothesis for olfactory receptors: Explanation of the differential binding of ketones to the mouse and human orthologs of olfactory receptor 912-93. Protein Science, 2005, 14, 703-710.	3.1	43
348	Improved Non-Pt Alloys for the Oxygen Reduction Reaction at Fuel Cell Cathodes Predicted from Quantum Mechanics. Journal of Physical Chemistry C, 2010, 114, 11527-11533.	1.5	43
349	Largeâ€scale, longâ€term nonadiabatic electron molecular dynamics for describing material properties and phenomena in extreme environments. Journal of Computational Chemistry, 2011, 32, 497-512.	1.5	43
350	Nucleation of amorphous shear bands at nanotwins in boron suboxide. Nature Communications, 2016, 7, 11001.	5.8	43
351	How the toughness in metallic glasses depends on topological and chemical heterogeneity. Proceedings of the National Academy of Sciences of the United States of America, 2016, 113, 7053-7058.	3.3	43
352	Polarizable charge equilibration model for predicting accurate electrostatic interactions in molecules and solids. Journal of Chemical Physics, 2017, 146, 124117.	1.2	43
353	Mechanism and kinetics of the electrocatalytic reaction responsible for the high cost of hydrogen fuel cells. Physical Chemistry Chemical Physics, 2017, 19, 2666-2673.	1.3	43
354	Predicted Structures of the Active Sites Responsible for the Improved Reduction of Carbon Dioxide by Gold Nanoparticles. Journal of Physical Chemistry Letters, 2017, 8, 3317-3320.	2.1	43
355	The chemical reactions in electrosprays of water do not always correspond to those at the pristine air–water interface. Chemical Science, 2019, 10, 2566-2577.	3.7	43
356	Electrochemical Switching of a Fluorescent Molecular Rotor Embedded within a Bistable Rotaxane. Journal of the American Chemical Society, 2020, 142, 11835-11846.	6.6	43
357	The DFT-ReaxFF Hybrid Reactive Dynamics Method with Application to the Reductive Decomposition Reaction of the TFSI and DOL Electrolyte at a Lithium–Metal Anode Surface. Journal of Physical Chemistry Letters, 2021, 12, 1300-1306.	2.1	43
358	A theoretical study of collision induced desorption spectroscopy from Si(111) surfaces. Journal of Chemical Physics, 1986, 84, 2408-2420.	1.2	42
359	Kinetic steps for α-helix formation. , 1998, 33, 343-357.		42
360	Atomic simulations of kinetic friction and its velocity dependence atAlâ^•Alandαâ^'Al2O3â^•αâ^'Al2O3interfaces. Physical Review B, 2005, 72, .	1.1	42

#	Article	IF	CITATIONS
361	Annealing kinetics of electrodeposited lithium dendrites. Journal of Chemical Physics, 2015, 143, 134701.	1.2	42
362	Boron Suboxide and Boron Subphosphide Crystals: Hard Ceramics That Shear without Brittle Failure. Chemistry of Materials, 2015, 27, 2855-2860.	3.2	42
363	Nanotwinned Boron Suboxide (B6O): New Ground State of B6O. Nano Letters, 2016, 16, 4236-4242.	4.5	42
364	Intramolecular Energy and Electron Transfer within a Diazaperopyrenium-Based Cyclophane. Journal of the American Chemical Society, 2017, 139, 4107-4116.	6.6	42
365	Locating Si atoms in Si-doped boron carbide: A route to understand amorphization mitigation mechanism. Acta Materialia, 2018, 157, 106-113.	3.8	42
366	Liquid water is a dynamic polydisperse branched polymer. Proceedings of the National Academy of Sciences of the United States of America, 2019, 116, 1998-2003.	3.3	42
367	Correlation Analysis of Chemical Bonds. Journal of Physical Chemistry A, 1998, 102, 2919-2933.	1.1	41
368	Heterogeneous Inhibition of Homogeneous Reactions:  Karstedt Catalyzed Hydrosilylation. Journal of Physical Chemistry B, 2002, 106, 1714-1721.	1.2	41
369	Characterization of the active site of yeast RNA polymerase II by DFT and ReaxFF calculations. Theoretical Chemistry Accounts, 2008, 120, 479-489.	0.5	41
370	Modeling High Rate Impact Sensitivity of Perfect RDX and HMX Crystals by ReaxFF Reactive Dynamics. Journal of Energetic Materials, 2010, 28, 92-127.	1.0	41
371	CO ₂ reduction on pure Cu produces only H ₂ after subsurface O is depleted: Theory and experiment. Proceedings of the National Academy of Sciences of the United States of America, 2021, 118, .	3.3	41
372	Pseudospectral contracted configuration interaction from a generalized valence bond reference. Journal of Chemical Physics, 1994, 101, 2986-2994.	1.2	40
373	Superprotonic phase transition ofCsHSO4: A molecular dynamics simulation study. Physical Review B, 2005, 72, .	1.1	40
374	ReaxFF Reactive Force-Field Modeling of the Triple-Phase Boundary in a Solid Oxide Fuel Cell. Journal of Physical Chemistry Letters, 2014, 5, 4039-4043.	2.1	40
375	Ligand- and mutation-induced conformational selection in the CCR5 chemokine G protein-coupled receptor. Proceedings of the National Academy of Sciences of the United States of America, 2014, 111, 13040-13045.	3.3	40
376	Accurate Ab Initio Quantum Mechanics Simulations of Bi ₂ Se ₃ and Bi ₂ Te ₃ Topological Insulator Surfaces. Journal of Physical Chemistry Letters, 2015, 6, 3792-3796.	2.1	40
377	Role of Ligand Protonation in Dihydrogen Evolution from a Pentamethylcyclopentadienyl Rhodium Catalyst. Inorganic Chemistry, 2017, 56, 11375-11386.	1.9	40
378	Mechanism of β-arrestin recruitment by the μ-opioid G protein-coupled receptor. Proceedings of the National Academy of Sciences of the United States of America, 2020, 117, 16346-16355.	3.3	40

#	Article	IF	CITATIONS
379	The Hessian biased singular value decomposition method for optimization and analysis of force fields. Journal of Chemical Physics, 1996, 104, 2898-2920.	1.2	39
380	Structures and Energetics Study of Tetrathiafulvalene-Based Donors of Organic Superconductors. Journal of Physical Chemistry A, 1997, 101, 8128-8131.	1.1	39
381	Atomistic Simulations of Corrosion Inhibitors Adsorbed on Calcite Surfaces I. Force field Parameters for Calcite. Journal of Physical Chemistry B, 2001, 105, 10746-10752.	1.2	39
382	First-Principles-Based Dispersion Augmented Density Functional Theory: From Molecules to Crystals. Journal of Physical Chemistry Letters, 2010, 1, 2550-2555.	2.1	39
383	Mechanism of efficient anti-Markovnikov olefin hydroarylation catalyzed by homogeneous Ir(<scp>iii</scp>) complexes. Green Chemistry, 2011, 13, 69-81.	4.6	39
384	Molecular basis for dramatic changes in cannabinoid CB1 G protein oupled receptor activation upon single and double point mutations. Protein Science, 2013, 22, 101-113.	3.1	39
385	Toward a Process-Based Molecular Model of SiC Membranes. 1. Development of a Reactive Force Field. Journal of Physical Chemistry C, 2013, 117, 3308-3319.	1.5	39
386	The Reduction-Coupled Oxo Activation (ROA) Mechanism Responsible for the Catalytic Selective Activation and Functionalization of n-Butane to Maleic Anhydride by Vanadium Phosphate Oxide. Topics in Catalysis, 2014, 57, 1171-1187.	1.3	39
387	Size-Matched Radical Multivalency. Journal of the American Chemical Society, 2017, 139, 3986-3998.	6.6	39
388	Fracture toughness of thermoelectric materials. Materials Science and Engineering Reports, 2021, 144, 100607.	14.8	39
389	Energetics of hydrogen coverage on group VIII transition metal surfaces and a kinetic model for adsorption/desorption. Journal of Chemical Physics, 2005, 122, 014704.	1.2	38
390	Use of G-Protein-Coupled and -Uncoupled CCR5 Receptors by CCR5 Inhibitor-Resistant and -Sensitive Human Immunodeficiency Virus Type 1 Variants. Journal of Virology, 2013, 87, 6569-6581.	1.5	38
391	SuperBiHelix method for predicting the pleiotropic ensemble of G-protein–coupled receptor conformations. Proceedings of the National Academy of Sciences of the United States of America, 2014, 111, E72-8.	3.3	38
392	Mechanisms Underlying the Mpemba Effect in Water from Molecular Dynamics Simulations. Journal of Physical Chemistry C, 2015, 119, 2622-2629.	1.5	38
393	Rescaling of metal oxide nanocrystals for energy storage having high capacitance and energy density with robust cycle life. Proceedings of the National Academy of Sciences of the United States of America, 2015, 112, 7914-7919.	3.3	38
394	Initial decomposition reaction of di-tetrazine-tetroxide (DTTO) from quantum molecular dynamics: implications for a promising energetic material. Journal of Materials Chemistry A, 2015, 3, 1972-1978.	5.2	38
395	A bitter pill for type 2 diabetes? The activation of bitter taste receptor TAS2R38 can stimulate GLP-1 release from enteroendocrine L-cells. Biochemical and Biophysical Research Communications, 2016, 475, 295-300.	1.0	38
396	The atomistic level structure for the activated human κ-opioid receptor bound to the full Gi protein and the MP1104 agonist. Proceedings of the National Academy of Sciences of the United States of America, 2020, 117, 5836-5843.	3.3	38

#	Article	IF	CITATIONS
397	Chromophore-in-Protein Modeling of the Structures and Resonance Raman Spectra for Type 1 Copper Proteins. Journal of the American Chemical Society, 1998, 120, 12791-12797.	6.6	37
398	Conformational Equilibria of β-Alanine and Related Compounds as Studied by NMR Spectroscopy. Journal of the American Chemical Society, 1998, 120, 7537-7543.	6.6	37
399	3-Dimensional Structures of G Protein-Coupled Receptors and Binding Sites of Agonists and Antagonists. Journal of Nutrition, 2007, 137, 1528S-1538S.	1.3	37
400	Improved H ₂ Storage in Zeolitic Imidazolate Frameworks Using Li ⁺ , Na ⁺ , and K ⁺ Dopants, with an Emphasis on Delivery H ₂ Uptake. Journal of Physical Chemistry C, 2011, 115, 3507-3512.	1.5	37
401	Structure-Based Prediction of Subtype Selectivity of Histamine H ₃ Receptor Selective Antagonists in Clinical Trials. Journal of Chemical Information and Modeling, 2011, 51, 3262-3274.	2.5	37
402	Density Functional Theory Study of Pt ₃ M Alloy Surface Segregation with Adsorbed O/OH and Pt ₃ Os as Catalysts for Oxygen Reduction Reaction. Journal of Physical Chemistry C, 2014, 118, 26703-26712.	1.5	37
403	Highly Selective Electrocatalytic Reduction of CO ₂ into Methane on Cu–Bi Nanoalloys. Journal of Physical Chemistry Letters, 2020, 11, 7261-7266.	2.1	37
404	Reaction Mechanism, Origins of Enantioselectivity, and Reactivity Trends in Asymmetric Allylic Alkylation: A Comprehensive Quantum Mechanics Investigation of a C(sp ³)–C(sp ³) Cross-Coupling. Journal of the American Chemical Society, 2020, 142, 13917-13933.	6.6	37
405	The Role of Confined Water in Ionic Liquid Electrolytes for Dye-Sensitized Solar Cells. Journal of Physical Chemistry Letters, 2012, 3, 556-559.	2.1	36
406	Computationallyâ€predicted CB1 cannabinoid receptor mutants show distinct patterns of saltâ€bridges that correlate with their level of constitutive activity reflected in G protein coupling levels, thermal stability, and ligand binding. Proteins: Structure, Function and Bioinformatics, 2013, 81, 1304-1317.	1.5	36
407	Mechanical-Bond-Protected, Air-Stable Radicals. Journal of the American Chemical Society, 2017, 139, 12704-12709.	6.6	36
408	Enhanced oxygen evolution catalyzed by <i>in situ</i> formed Fe-doped Ni oxyhydroxides in carbon nanotubes. Journal of Materials Chemistry A, 2022, 10, 16007-16015.	5.2	36
409	Parametrization of a reactive force field for aluminum hydride. Journal of Chemical Physics, 2009, 131, 044501.	1.2	35
410	Functionalization of Rhenium Aryl Bonds by O-Atom Transfer. Organometallics, 2011, 30, 2079-2082.	1.1	35
411	Chemistry in the Center for Catalytic Hydrocarbon Functionalization: An Energy Frontier Research Center. Catalysis Letters, 2011, 141, 213-221.	1.4	35
412	Branched Polymeric Media: Boron-Chelating Resins from Hyperbranched Polyethylenimine. Environmental Science & Technology, 2012, 46, 8998-9004.	4.6	35
413	Prediction of the Chapman–Jouguet chemical equilibrium state in a detonation wave from first principles based reactive molecular dynamics. Physical Chemistry Chemical Physics, 2016, 18, 2015-2022.	1.3	35
414	Regulating Top‣urface Multilayer/Singleâ€Crystal Graphene Growth by "Gettering―Carbon Diffusion at Backside of the Copper Foil. Advanced Functional Materials, 2017, 27, 1700121.	7.8	35

#	Article	IF	CITATIONS
415	Multilayer Two-Dimensional Water Structure Confined in MoS ₂ . Journal of Physical Chemistry C, 2017, 121, 16021-16028.	1.5	35
416	Electrocatalytic Water Oxidation by a Trinuclear Copper(II) Complex. ACS Catalysis, 2021, 11, 7223-7240.	5.5	35
417	Can the Monomer of the Leucine Zipper Proteins Recognize the Dimer Binding Site without Dimerization?. Journal of the American Chemical Society, 1996, 118, 4235-4239.	6.6	34
418	Competing, Coverage-Dependent Decomposition Pathways for C ₂ H _{<i>y</i>} Species on Nickel (111). Journal of Physical Chemistry C, 2010, 114, 20028-20041.	1.5	34
419	Shock response of a model structured nanofoam of Cu. Journal of Applied Physics, 2013, 113, .	1.1	34
420	Shock response of single crystal and nanocrystalline pentaerythritol tetranitrate: Implications to hotspot formation in energetic materials. Journal of Chemical Physics, 2013, 139, 164704.	1.2	34
421	Interaction of e. coli outer-membrane protein A with sugars on the receptors of the brain microvascular endothelial cells. Proteins: Structure, Function and Bioinformatics, 2002, 50, 213-221.	1.5	33
422	Application of the COSMOâ^'SACâ^'BP Solvation Model to Predictions of Normal Boiling Temperatures for Environmentally Significant Substances. Industrial & Engineering Chemistry Research, 2006, 45, 5426-5434.	1.8	33
423	Predicted Optimum Composition for the Glass-Forming Ability of Bulk Amorphous Alloys: Application to Cu–Zr–Al. Journal of Physical Chemistry Letters, 2012, 3, 3143-3148.	2.1	33
424	Sliding-Ring Catenanes. Journal of the American Chemical Society, 2016, 138, 10214-10225.	6.6	33
425	Selectivity for HCO ₂ [–] over H ₂ in the Electrochemical Catalytic Reduction of CO ₂ by (POCOP)IrH ₂ . ACS Catalysis, 2016, 6, 6362-6371.	5.5	33
426	CO Coupling Chemistry of a Terminal Mo Carbide: Sequential Addition of Proton, Hydride, and CO Releases Ethenone. Journal of the American Chemical Society, 2019, 141, 15664-15674.	6.6	33
427	Autobifunctional Mechanism of Jagged Pt Nanowires for Hydrogen Evolution Kinetics via End-to-End Simulation. Journal of the American Chemical Society, 2021, 143, 5355-5363.	6.6	33
428	The structure of human serotonin 2c G-protein-coupled receptor bound to agonists and antagonists. Journal of Molecular Graphics and Modelling, 2008, 27, 66-81.	1.3	32
429	Dynamic response of phenolic resin and its carbon-nanotube composites to shock wave loading. Journal of Applied Physics, 2011, 109, 013503.	1.1	32
430	Interfacial Thermodynamics of Water and Six Other Liquid Solvents. Journal of Physical Chemistry B, 2014, 118, 5943-5956.	1.2	32
431	Solid-State Characterization and Photoinduced Intramolecular Electron Transfer in a Nanoconfined Octacationic Homo[2]Catenane. Journal of the American Chemical Society, 2014, 136, 10569-10572.	6.6	32
432	QM-Mechanism-Based Hierarchical High-Throughput in Silico Screening Catalyst Design for Ammonia Synthesis. Journal of the American Chemical Society, 2018, 140, 17702-17710.	6.6	32

#	Article	IF	CITATIONS
433	Effects of High and Low Salt Concentrations in Electrolytes at Lithium–Metal Anode Surfaces Using DFT-ReaxFF Hybrid Molecular Dynamics Method. Journal of Physical Chemistry Letters, 2021, 12, 2922-2929.	2.1	32
434	Chemisorption of oxygen and aluminum on the GaAs (110) surface from ab initio theory. Journal of Vacuum Science and Technology, 1980, 17, 164-168.	1.9	31
435	The continuous configurational Boltzmann biased direct Monte Carlo method for free energy properties of polymer chains. Journal of Chemical Physics, 1997, 106, 6722-6729.	1.2	31
436	Ab initioevidence for the formation of impurityd3z2â^'r2holes in dopedLa2â^'xSrxCuO4. Physical Review B, 2002, 65, .	1.1	31
437	Nanopores of carbon nanotubes as practical hydrogen storage media. Applied Physics Letters, 2005, 87, 213113.	1.5	31
438	Breaking the icosahedra in boron carbide. Proceedings of the National Academy of Sciences of the United States of America, 2016, 113, 12012-12016.	3.3	31
439	Deformation mechanisms in high-efficiency thermoelectric layered Zintl compounds. Journal of Materials Chemistry A, 2017, 5, 9050-9059.	5.2	31
440	Interface Structure in Li-Metal/[Pyr ₁₄][TFSI]-Ionic Liquid System from ab Initio Molecular Dynamics Simulations. Journal of Physical Chemistry Letters, 2019, 10, 4577-4586.	2.1	31
441	Liquefaction of H2 molecules upon exterior surfaces of carbon nanotube bundles. Applied Physics Letters, 2005, 86, 203108.	1.5	30
442	Origin of static friction and its relationship to adhesion at the atomic scale. Physical Review B, 2007, 75, .	1.1	30
443	Predicted structures of agonist and antagonist bound complexes of adenosine A ₃ receptor. Proteins: Structure, Function and Bioinformatics, 2011, 79, 1878-1897.	1.5	30
444	Prediction of the Dependence of the Fuel Cell Oxygen Reduction Reactions on Operating Voltage from DFT Calculations. Journal of Physical Chemistry C, 2012, 116, 6166-6173.	1.5	30
445	Nanocomposites of Tantalumâ€Based Pyrochlore and Indium Hydroxide Showing High and Stable Photocatalytic Activities for Overall Water Splitting and Carbon Dioxide Reduction. Angewandte Chemie - International Edition, 2014, 53, 14216-14220.	7.2	30
446	Mechanisms and energetics of free radical initiated disulfide bond cleavage in model peptides and insulin by mass spectrometry. Chemical Science, 2015, 6, 4550-4560.	3.7	30
447	Nanotwins soften boron-rich boron carbide (B13C2). Applied Physics Letters, 2017, 110, .	1.5	30
448	Dramatically reduced lattice thermal conductivity of Mg2Si thermoelectric material from nanotwinning. Acta Materialia, 2019, 169, 9-14.	3.8	30
449	Photochemically deposited Ir-doped NiCo oxyhydroxide nanosheets provide highly efficient and stable electrocatalysts for the oxygen evolution reaction. Nano Energy, 2020, 75, 104885.	8.2	30
450	Dissociation energetics of SiF systems of relevance to etching reactions. Journal of Chemical Physics, 1987, 87, 1307-1314.	1.2	29

#	Article	IF	CITATIONS
451	MSX Force Field and Vibrational Frequencies for BEDT-TTF (Neutral and Cation). Journal of Physical Chemistry A, 1997, 101, 1975-1981.	1.1	29
452	Ab Initio Investigation of Ethane Dissociation Using Generalized Transition State Theory. Journal of Physical Chemistry A, 2001, 105, 7896-7904.	1.1	29
453	Tropospheric aerosol as a reactive intermediate. Faraday Discussions, 2013, 165, 407.	1.6	29
454	Influence of Constitution and Charge on Radical Pairing Interactions in Tris-radical Tricationic Complexes. Journal of the American Chemical Society, 2016, 138, 8288-8300.	6.6	29
455	The Oxygen Reduction Reaction on Graphene from Quantum Mechanics: Comparing Armchair and Zigzag Carbon Edges. Journal of Physical Chemistry C, 2017, 121, 24408-24417.	1.5	29
456	First-principles–based reaction kinetics from reactive molecular dynamics simulations: Application to hydrogen peroxide decomposition. Proceedings of the National Academy of Sciences of the United States of America, 2019, 116, 18202-18208.	3.3	29
457	Artificial Intelligence and QM/MM with a Polarizable Reactive Force Field for Next-Generation Electrocatalysts. Matter, 2021, 4, 195-216.	5.0	29
458	Approaching 100% Selectivity at Low Potential on Ag for Electrochemical CO ₂ Reduction to CO Using a Surface Additive. ACS Catalysis, 2021, 11, 9034-9042.	5.5	29
459	A generalized direct inversion in the iterative subspace approach for generalized valence bond wave functions. Journal of Chemical Physics, 1994, 100, 1226-1235.	1.2	28
460	The MPSim-Dock hierarchical docking algorithm: Application to the eight trypsin inhibitor cocrystals. Journal of Computational Chemistry, 2005, 26, 48-71.	1.5	28
461	ReaxFF Monte Carlo reactive dynamics: Application to resolving the partial occupations of the M1 phase of the MoVNbTeO catalyst. Catalysis Today, 2010, 157, 71-76.	2.2	28
462	Predicted Structures and Dynamics for Agonists and Antagonists Bound to Serotonin 5-HT2B and 5-HT2C Receptors. Journal of Chemical Information and Modeling, 2011, 51, 420-433.	2.5	28
463	p-Type Co Interstitial Defects in Thermoelectric Skutterudite CoSb ₃ Due to the Breakage of Sb ₄ -Rings. Chemistry of Materials, 2016, 28, 2172-2179.	3.2	28
464	Atomistic explanation of brittle failure of thermoelectric skutterudite CoSb3. Acta Materialia, 2016, 103, 775-780.	3.8	28
465	Initial Decomposition of HMX Energetic Material from Quantum Molecular Dynamics and the Molecular Structure Transition of β-HMX to δ-HMX. Journal of Physical Chemistry C, 2019, 123, 9231-9236.	1.5	28
466	Si-Doped Fe Catalyst for Ammonia Synthesis at Dramatically Decreased Pressures and Temperatures. Journal of the American Chemical Society, 2020, 142, 8223-8232.	6.6	28
467	Machine learning for design principles for single atom catalysts towards electrochemical reactions. Journal of Materials Chemistry A, 2022, 10, 15309-15331.	5.2	28
468	Ab Initio Calculations on the H2 + D2 → 2HD Four enter Exchange Reaction. II. Orbitals, Contragradience, and the Reaction Surface. Journal of Chemical Physics, 1972, 56, 5913-5920.	1.2	27

#	Article	IF	CITATIONS
469	First principles studies of band offsets at heterojunctions and of surface reconstruction using Gaussian dual-space density functional theory. Journal of Vacuum Science & Technology an Official Journal of the American Vacuum Society B, Microelectronics Processing and Phenomena, 1995, 13, 1715.	1.6	27
470	Branched Polymeric Media: Perchlorate-Selective Resins from Hyperbranched Polyethyleneimine. Environmental Science & Technology, 2012, 46, 10718-10726.	4.6	27
471	Long-Range C–H Bond Activation by Rh ^{III} -Carboxylates. Journal of the American Chemical Society, 2014, 136, 14690-14693.	6.6	27
472	Improved Ductility of Boron Carbide by Microalloying with Boron Suboxide. Journal of Physical Chemistry C, 2015, 119, 24649-24656.	1.5	27
473	Predicting glycosaminoglycan surface protein interactions and implications for studying axonal growth. Proceedings of the National Academy of Sciences of the United States of America, 2017, 114, 13697-13702.	3.3	27
474	The quantum mechanics-based polarizable force field for water simulations. Journal of Chemical Physics, 2018, 149, 174502.	1.2	27
475	Reaction mechanism and kinetics for ammonia synthesis on the Fe(211) reconstructed surface. Physical Chemistry Chemical Physics, 2019, 21, 11444-11454.	1.3	27
476	The valenceâ€bond chargeâ€transferâ€exciton model for predicting nonlinear optical properties (hyperpolarizabilities and saturation length) of polymeric materials. Journal of Chemical Physics, 1994, 101, 4920-4930.	1.2	26
477	Fast Ewald sums for general van der Waals potentials. Journal of Computational Chemistry, 1997, 18, 1365-1370.	1.5	26
478	Catalytic Synthesis of Superlinear Alkenyl Arenes Using a Rh(I) Catalyst Supported by a "Capping Arene― Ligand: Access to Aerobic Catalysis. Journal of the American Chemical Society, 2018, 140, 17007-17018.	6.6	26
479	Selective Activation of Propane Using Intermediates Generated during Water Oxidation. Journal of the American Chemical Society, 2021, 143, 3967-3974.	6.6	26
480	Sulfur-doped graphene anchoring of ultrafine Au25 nanoclusters for electrocatalysis. Nano Research, 2021, 14, 3509-3513.	5.8	26
481	Arene C–H activation using Rh(<scp>i</scp>) catalysts supported by bidentate nitrogen chelates. Catalysis Science and Technology, 2015, 5, 96-100.	2.1	25
482	Mechanical properties in thermoelectric oxides: Ideal strength, deformation mechanism, and fracture toughness. Acta Materialia, 2018, 149, 341-349.	3.8	25
483	The mechanism for ligand activation of the GPCR–G protein complex. Proceedings of the National Academy of Sciences of the United States of America, 2022, 119, e2110085119.	3.3	25
484	Methane Functionalization. , 2006, , 235-285.		24
485	Prediction of the 3D Structure of FMRFâ€amide Neuropeptides Bound to the Mouse MrgC11 GPCR and Experimental Validation. ChemBioChem, 2007, 8, 1527-1539.	1.3	24
486	Toward a Process-Based Molecular Model of SiC Membranes. 2. Reactive Dynamics Simulation of the Pyrolysis of Polymer Precursor To Form Amorphous SiC. Journal of Physical Chemistry C, 2013, 117, 3320-3329.	1.5	24

#	Article	IF	CITATIONS
487	DFT Virtual Screening Identifies Rhodium–Amidinate Complexes As Potential Homogeneous Catalysts for Methane-to-Methanol Oxidation. ACS Catalysis, 2014, 4, 4455-4465.	5.5	24
488	Rhodium Bis(quinolinyl)benzene Complexes for Methane Activation and Functionalization. Chemistry - A European Journal, 2015, 21, 1286-1293.	1.7	24
489	Pressureâ€Dependent Polymorphism and Bandâ€Gap Tuning of Methylammonium Lead Iodide Perovskite. Angewandte Chemie, 2016, 128, 6650-6654.	1.6	24
490	Prediction of the crystal packing of diâ€ŧetrazineâ€ŧetroxide (DTTO) energetic material. Journal of Computational Chemistry, 2016, 37, 163-167.	1.5	24
491	Synthesis and structure-activity relationships of quinolinone and quinoline-based P2X7 receptor antagonists and their anti-sphere formation activities in glioblastoma cells. European Journal of Medicinal Chemistry, 2018, 151, 462-481.	2.6	24
492	Predicted Operando Polymerization at Lithium Anode via Boron Insertion. ACS Energy Letters, 2021, 6, 2320-2327.	8.8	24
493	The theoretical determination of the B 1Îu potential energy curve for Li2. Journal of Chemical Physics, 1977, 66, 1135-1140.	1.2	23
494	Computational Materials Chemistry at the Nanoscale. Journal of Nanoparticle Research, 1999, 1, 51-69.	0.8	23
495	Simulations on the effects of confinement and Ni-catalysis on the formation of tubular fullerene structures from peapod precursors. Physical Review B, 2007, 75, .	1.1	23
496	Efficiency of Ï€â^'Ï€ Tunneling in [2]Rotaxane Molecular Electronic Switches. Journal of Physical Chemistry C, 2007, 111, 4831-4837.	1.5	23
497	Mechanisms of Auger-induced chemistry derived from wave packet dynamics. Proceedings of the National Academy of Sciences of the United States of America, 2009, 106, 1001-1005.	3.3	23
498	Hypervelocity Impact Effect of Molecules from Enceladus' Plume and Titan's Upper Atmosphere on NASA's Cassini Spectrometer from Reactive Dynamics Simulation. Physical Review Letters, 2012, 109, 213201.	2.9	23
499	Synthesis of single-component metallic glasses by thermal spray of nanodroplets on amorphous substrates. Applied Physics Letters, 2012, 100, .	1.5	23
500	Structure Prediction of G Protein-Coupled Receptors and Their Ensemble of Functionally Important Conformations. Methods in Molecular Biology, 2012, 914, 237-254.	0.4	23
501	Dependence on the structure and surface polarity of ZnS photocatalytic activities of water splitting: first-principles calculations. Physical Chemistry Chemical Physics, 2013, 15, 9531.	1.3	23
502	Catalytic activity of Pt ₃₈ in the oxygen reduction reaction from first-principles simulations. Catalysis Science and Technology, 2016, 6, 6901-6909.	2.1	23
503	Mechanism of Hydrocarbon Functionalization by an Iodate/Chloride System: The Role of Ester Protection. ACS Catalysis, 2018, 8, 3138-3149.	5.5	23
504	Accurate non-bonded potentials based on periodic quantum mechanics calculations for use in molecular simulations of materials and systems. Journal of Chemical Physics, 2019, 151, 154111.	1.2	23

#	Article	IF	CITATIONS
505	Formation of two glass phases in binary Cu-Ag liquid. Acta Materialia, 2020, 195, 274-281.	3.8	23
506	Performance of electrochemical immunoassays for clinical diagnostics of SARS-CoV-2 based on selective nucleocapsid N protein detection: Boron-doped diamond, gold and glassy carbon evaluation. Biosensors and Bioelectronics, 2022, 209, 114222.	5.3	23
507	Reaction Mechanisms, Kinetics, and Improved Catalysts for Ammonia Synthesis from Hierarchical High Throughput Catalyst Design. Accounts of Chemical Research, 2022, 55, 1124-1134.	7.6	23
508	De novo prediction of polypeptide conformations using dihedral probability grid Monte Carlo methodology. Protein Science, 1995, 4, 1203-1216.	3.1	22
509	Structures, Mechanisms, and Kinetics of Ammoxidation and Selective Oxidation of Propane Over the M2 Phase of MoVNbTeO Catalysts. Topics in Catalysis, 2011, 54, 659-668.	1.3	22
510	Shock-induced consolidation and spallation of Cu nanopowders. Journal of Applied Physics, 2012, 111, .	1.1	22
511	Rapid Dye Regeneration Mechanism of Dye-Sensitized Solar Cells. Journal of Physical Chemistry Letters, 2014, 5, 4285-4290.	2.1	22
512	Inhibition of Hotspot Formation in Polymer Bonded Explosives Using an Interface Matching Low Density Polymer Coating at the Polymer–Explosive Interface. Journal of Physical Chemistry C, 2014, 118, 19918-19928.	1.5	22
513	Neighboring Component Effect in a Tri-stable [2]Rotaxane. Journal of the American Chemical Society, 2018, 140, 13827-13834.	6.6	22
514	Growth and Isolation of Large Area Boronâ€Doped Nanocrystalline Diamond Sheets: A Route toward Diamondâ€onâ€Graphene Heterojunction. Advanced Functional Materials, 2019, 29, 1805242.	7.8	22
515	Sulfated glycans engage the Ang–Tie pathway to regulate vascular development. Nature Chemical Biology, 2021, 17, 178-186.	3.9	22
516	Selective Enhancement of Methane Formation in Electrochemical CO ₂ Reduction Enabled by a Raman-Inactive Oxygen-Containing Species on Cu. ACS Catalysis, 2022, 12, 6036-6046.	5.5	22
517	Spinâ€Generalized SCF Wavefunctions for H2O, OH, and O. Journal of Chemical Physics, 1970, 53, 1803-1814.	1.2	21
518	Activated Complex Theory of Barite Scale Control Processes. Molecular Engineering, 1997, 7, 491-514.	0.2	21
519	ReaxFF reactive molecular dynamics on silicon pentaerythritol tetranitrate crystal validates the mechanism for the colossal sensitivity. Physical Chemistry Chemical Physics, 2014, 16, 23779-23791.	1.3	21
520	Shear-Induced Brittle Failure along Grain Boundaries in Boron Carbide. ACS Applied Materials & Interfaces, 2018, 10, 5072-5080.	4.0	21
521	Predicted detonation properties at the Chapman–Jouguet state for proposed energetic materials (MTO) Tj ETC Chemical Physics, 2018, 20, 3953-3969.	Qq1 1 0.78 1.3	34314 rgBT 0 21
522	Effects of Lewis Acidic Metal Ions (M) on Oxygen-Atom Transfer Reactivity of Heterometallic Mn ₃ MO ₄ Cubane and Fe ₃ MO(OH) and Mn ₃ MO(OH) Clusters. Inorganic Chemistry, 2019, 58, 2336-2345.	1.9	21

#	Article	IF	CITATIONS
523	Role of Ferryl Ion Intermediates in Fast Fenton Chemistry on Aqueous Microdroplets. Environmental Science & Technology, 2021, 55, 14370-14377.	4.6	21
524	Effects of pressure on the structure of metmyoglobin: Molecular dynamics predictions for pressure unfolding through a molten globule intermediate. Protein Science, 1998, 7, 2301-2313.	3.1	20
525	Optimizing the oxygen evolution reaction for electrochemical water oxidation by tuning solvent properties. Nanoscale, 2015, 7, 4514-4521.	2.8	20
526	The Mechanism of Alkane Selective Oxidation by the M1 Phase of Mo–V–Nb–Te Mixed Metal Oxides: Suggestions for Improved Catalysts. Topics in Catalysis, 2016, 59, 1506-1517.	1.3	20
527	pH-Dependent Conformations for Hyperbranched Poly(ethylenimine) from All-Atom Molecular Dynamics. Macromolecules, 2018, 51, 2187-2194.	2.2	20
528	First-Order Phase Transition in Liquid Ag to the Heterogeneous G-Phase. Journal of Physical Chemistry Letters, 2020, 11, 632-645.	2.1	20
529	Orbital Description and Properties of the BH Molecule. Journal of Chemical Physics, 1972, 57, 5296-5310.	1.2	19
530	Vibrational Analysis and Isotope Shifts of BEDT-TTF Donor for Organic Superconductors. Journal of Physical Chemistry A, 1998, 102, 2466-2471.	1.1	19
531	Solvent Effects on the Secondary Structures of Proteins. Journal of Physical Chemistry A, 2000, 104, 2498-2503.	1.1	19
532	Mechanism of Selective Ammoxidation of Propene to Acrylonitrile on Bismuth Molybdates from Quantum Mechanical Calculations. Journal of Physical Chemistry C, 2010, 114, 15678-15694.	1.5	19
533	Origin of the Pseudogap in High-Temperature Cuprate Superconductors. Journal of Physical Chemistry Letters, 2011, 2, 2326-2330.	2.1	19
534	Interface dynamics: Mechanisms of stabilization and destabilization and structure of flow fields. Proceedings of the National Academy of Sciences of the United States of America, 2019, 116, 18218-18226.	3.3	19
535	Initial Steps in Forming the Electrode–Electrolyte Interface: H2O Adsorption and Complex Formation on the Ag(111) Surface from Combining Quantum Mechanics Calculations and Ambient Pressure X-ray Photoelectron Spectroscopy. Journal of the American Chemical Society, 2019, 141, 6946-6954.	6.6	19
536	Synergy between a Silver–Copper Surface Alloy Composition and Carbon Dioxide Adsorption and Activation. ACS Applied Materials & Interfaces, 2020, 12, 25374-25382.	4.0	19
537	Classical Stochastic Diffusion Theory for Desorption of Atoms and Molecules from Solid Surfaces. Physical Review Letters, 1982, 49, 1847-1850.	2.9	18
538	Atomistic simulations of the LaMnO3 (110) polar surface. Physical Chemistry Chemical Physics, 2003, 5, 4180.	1.3	18
539	Lancifodilactone G: Insights about an Unusually Stable Enol. Journal of Organic Chemistry, 2008, 73, 6853-6856.	1.7	18
540	Quantum mechanics based force field for carbon (QMFF-Cx) validated to reproduce the mechanical and thermodynamics properties of graphite. Journal of Chemical Physics, 2010, 133, 134114.	1.2	18

#	Article	IF	CITATIONS
541	Thermodynamics of Water Stabilization of Carboxybetaine Hydrogels from Molecular Dynamics Simulations. Journal of Physical Chemistry Letters, 2011, 2, 1757-1760.	2.1	18
542	Activation and Oxidation of Mesitylene C–H Bonds by (Phebox)Iridium(III) Complexes. Organometallics, 2015, 34, 2879-2888.	1.1	18
543	Reaction mechanism from quantum molecular dynamics for the initial thermal decomposition of 2,4,6-triamino-1,3,5-triazine-1,3,5-trioxide (MTO) and 2,4,6-trinitro-1,3,5-triazine-1,3,5-trioxide (MTO3N), promising green energetic materials. Journal of Materials Chemistry A, 2015, 3, 12044-12050.	5.2	18
544	Conformational and Thermodynamic Landscape of GPCR Activation from Theory and Computation. Biophysical Journal, 2016, 110, 2618-2629.	0.2	18
545	Ductility in Crystalline Boron Subphosphide (B ₁₂ P ₂) for Large Strain Indentation. Journal of Physical Chemistry C, 2017, 121, 16644-16649.	1.5	18
546	Mixed-Valence Superstructure Assembled from a Mixed-Valence Host–Guest Complex. Journal of the American Chemical Society, 2018, 140, 9387-9391.	6.6	18
547	Finite-pulse waves for efficient suppression of evolving mesoscale dendrites in rechargeable batteries. Physical Review E, 2019, 100, 042801.	0.8	18
548	Interfaces and mixing: Nonequilibrium transport across the scales. Proceedings of the National Academy of Sciences of the United States of America, 2019, 116, 18171-18174.	3.3	18
549	Structures and reactivity of neutral and cationic molybdenum methylidene complexes. Organometallics, 1989, 8, 1550-1558.	1.1	17
550	The Mechanism by Which Ionic Liquids Enable Shilov-Type CH Activation in an Oxidizing Medium. Organometallics, 2008, 27, 3770-3773.	1.1	17
551	Time dependent behavior of a localized electron at a heterojunction boundary of graphene. Applied Physics Letters, 2010, 97, 043504.	1.5	17
552	Role of Specific Cations and Water Entropy on the Stability of Branched DNA Motif Structures. Journal of Physical Chemistry B, 2012, 116, 12159-12167.	1.2	17
553	Scaled Effective Solvent Method for Predicting the Equilibrium Ensemble of Structures with Analysis of Thermodynamic Properties of Amorphous Polyethylene Glycol–Water Mixtures. Journal of Physical Chemistry B, 2013, 117, 916-927.	1.2	17
554	A homolytic oxy-functionalization mechanism: intermolecular hydrocarbyl migration from M–R to vanadate oxo. Chemical Communications, 2014, 50, 10994-10996.	2.2	17
555	Initial Decomposition Reactions of Bicyclo-HMX [BCHMX or <i>cis</i> -1,3,4,6-Tetranitrooctahydroimidazo-[4,5- <i>d</i>]imidazole] from Quantum Molecular Dynamics Simulations. Journal of Physical Chemistry C, 2015, 119, 2290-2296.	1.5	17
556	Transition-Metal-Mediated Nucleophilic Aromatic Substitution with Acids. Organometallics, 2016, 35, 2053-2056.	1.1	17
557	Prediction of structures and properties of 2,4,6-triamino-1,3,5-triazine-1,3,5-trioxide (MTO) and 2,4,6-trinitro-1,3,5-triazine-1,3,5-trioxide (MTO3N) green energetic materials from DFT and ReaxFF molecular modeling. Journal of Materials Chemistry A, 2016, 4, 1264-1276.	5.2	17
558	Defect-Controlled Electronic Structure and Phase Stability in Thermoelectric Skutterudite CoSb ₃ . Chemistry of Materials, 2017, 29, 3999-4007.	3.2	17

#	Article	IF	CITATIONS
559	Factors affecting cyclic durability of all-solid-state lithium batteries using poly(ethylene oxide)-based polymer electrolytes and recommendations to achieve improved performance. Physical Chemistry Chemical Physics, 2018, 20, 26098-26104.	1.3	17
560	Highly Stable Organic Bisradicals Protected by Mechanical Bonds. Journal of the American Chemical Society, 2020, 142, 7190-7197.	6.6	17
561	Novel interaction between neurotrophic factor-α1/carboxypeptidase E and serotonin receptor, 5-HTR1E, protects human neurons against oxidative/neuroexcitotoxic stress via β-arrestin/ERK signaling. Cellular and Molecular Life Sciences, 2022, 79, 1.	2.4	17
562	Fidelity of Phenylalanyl-tRNA Synthetase in Binding the Natural Amino Acids. Journal of Physical Chemistry B, 2003, 107, 11549-11557.	1.2	16
563	Design and validation of non-metal oxo complexes for C–H activation. Chemical Communications, 2014, 50, 1748.	2.2	16
564	Predicted Structures for Kappa Opioid G-Protein Coupled Receptor Bound to Selective Agonists. Journal of Chemical Information and Modeling, 2015, 55, 614-627.	2.5	16
565	Epitaxial growth of cobalt oxide phases on Ru(0001) for spintronic device applications. Semiconductor Science and Technology, 2017, 32, 095011.	1.0	16
566	Highly Efficient Ni-Doped Iron Catalyst for Ammonia Synthesis from Quantum-Mechanics-Based Hierarchical High-Throughput Catalyst Screening. Journal of Physical Chemistry C, 2019, 123, 17375-17383.	1.5	16
567	Light irradiation induced brittle-to-ductile and ductile-to-brittle transition in inorganic semiconductors. Physical Review B, 2019, 99, .	1.1	16
568	Electronic Structural Origin of the Catalytic Activity Trend of Transition Metals for Electrochemical Nitrogen Reduction. Journal of Physical Chemistry C, 2019, 123, 31026-31031.	1.5	16
569	Shear induced deformation twinning evolution in thermoelectric InSb. Npj Computational Materials, 2021, 7, .	3.5	16
570	Orbital Description of the Excited States of LiH. Journal of Chemical Physics, 1972, 56, 3348-3359.	1.2	15
571	Building proteins from <i>C_α</i> coordinates using the dihedral probability grid Monte Carlo method. Protein Science, 1995, 4, 1217-1232.	3.1	15
572	Prediction of polyelectrolyte polypeptide structures using Monte Carlo conformational search methods with implicit solvation modeling. Protein Science, 1995, 4, 2019-2031.	3.1	15
573	Thermodynamic Properties of Asphaltenes Through Computer Assisted Structure Elucidation and Atomistic Simulations. 1. Bulk Arabian Light Asphaltenes. Petroleum Science and Technology, 2004, 22, 877-899.	0.7	15
574	First-Principles Based Approaches to Nano-Mechanical and Biomimetic Characterization of Polymer-Based Hydrogel Networks for Cartilage Scaffold-Supported Therapies. Journal of Computational and Theoretical Nanoscience, 2010, 7, 1238-1256.	0.4	15
575	Left-right loading dependence of shock response of (111)//(112) Cu bicrystals: Deformation and spallation. Journal of Applied Physics, 2012, 111, .	1.1	15
576	Conformational Ensemble View of G Protein-Coupled Receptors and the Effect of Mutations and Ligand Binding. Methods in Enzymology, 2013, 520, 31-48.	0.4	15

#	Article	IF	CITATIONS
577	Analytic Derivatives of Quartic-Scaling Doubly Hybrid XYGJ-OS Functional: Theory, Implementation, and Benchmark Comparison with M06-2X and MP2 Geometries for Nonbonded Complexes. Journal of Chemical Theory and Computation, 2013, 9, 1971-1976.	2.3	15
578	First-Principles Modeling of Ni ₄ M (M = Co, Fe, and Mn) Alloys as Solid Oxide Fuel Cell Anode Catalyst for Methane Reforming. Journal of Physical Chemistry C, 2016, 120, 207-214.	1.5	15
579	Structure and Properties of Boron-Very-Rich Boron Carbides: B ₁₂ Icosahedra Linked through Bent CBB Chains. Journal of Physical Chemistry C, 2018, 122, 2448-2453.	1.5	15
580	Use of Ligand Steric Properties to Control the Thermodynamics and Kinetics of Oxidative Addition and Reductive Elimination with Pincer-Ligated Rh Complexes. Organometallics, 2020, 39, 1917-1933.	1.1	15
581	Domain Motions in Phosphoglycerate Kinase using Hierarchical NEIMO Molecular Dynamics Simulations. Journal of Physical Chemistry A, 2000, 104, 2375-2383.	1.1	14
582	Ab Initio Studies On Phase Behavior of Barium Titanate. Materials Research Society Symposia Proceedings, 2002, 718, 1.	0.1	14
583	The magnetic and electronic structure of vanadyl pyrophosphate from density functional theory. Physical Chemistry Chemical Physics, 2011, 13, 9831.	1.3	14
584	Quantum chemical insights into the dissociation of nitric acid on the surface of aqueous electrolytes. International Journal of Quantum Chemistry, 2013, 113, 413-417.	1.0	14
585	The Interaction of N-Glycans in Fcl ³ Receptor I α-Chain with Escherichia coli K1 Outer Membrane Protein A for Entry into Macrophages. Journal of Biological Chemistry, 2014, 289, 30937-30949.	1.6	14
586	Predicted 3D structures of olfactory receptors with details of odorant binding to OR1G1. Journal of Computer-Aided Molecular Design, 2014, 28, 1175-1190.	1.3	14
587	Theoretical and Experimental Studies of the Dechlorination Mechanism of Carbon Tetrachloride on a Vivianite Ferrous Phosphate Surface. Journal of Physical Chemistry A, 2015, 119, 5714-5722.	1.1	14
588	Dual-Phase Mechanism for the Catalytic Conversion of <i>n</i> Butane to Maleic Anhydride by the Vanadyl Pyrophosphate Heterogeneous Catalyst. Journal of Physical Chemistry C, 2017, 121, 24069-24076.	1.5	14
589	Electrophilic RhI catalysts for arene H/D exchange in acidic media: Evidence for an electrophilic aromatic substitution mechanism. Journal of Molecular Catalysis A, 2017, 426, 381-388.	4.8	14
590	Extension of the Polarizable Charge Equilibration Model to Higher Oxidation States with Applications to Ge, As, Se, Br, Sn, Sb, Te, I, Pb, Bi, Po, and At Elements. Journal of Physical Chemistry A, 2018, 122, 639-645.	1.1	14
591	First principles predicting enhanced ductility of boride carbide through magnesium microalloying. Journal of the American Ceramic Society, 2019, 102, 5514-5523.	1.9	14
592	Reaction Mechanism and Strategy for Optimizing the Hydrogen Evolution Reaction on Single-Layer 1T′ WSe ₂ and WTe ₂ Based on Grand Canonical Potential Kinetics. ACS Applied Materials & Interfaces, 2021, 13, 55611-55620.	4.0	14
593	Reaction Kinetics of a Selected Number of Elementary Processes Involved in the Thermal Decomposition of 9-Methylphenanthrene Using Density Functional Theory. Journal of Physical Chemistry A, 2004, 108, 10302-10310.	1.1	13
594	Rhodium complexes bearing tetradentate diamine-bis(phenolate) ligands. Dalton Transactions, 2011, 40, 301-304.	1.6	13

#	Article	IF	CITATIONS
595	Structure and Failure Mechanism of the Thermoelectric CoSb ₃ /TiCoSb Interface. ACS Applied Materials & Interfaces, 2016, 8, 31968-31977.	4.0	13
596	Improved Ductility of B ₁₂ Icosahedra-based Superhard Materials through Icosahedral Slip. Journal of Physical Chemistry C, 2017, 121, 11831-11838.	1.5	13
597	The 3D Structure of Human DP Prostaglandin G-Protein-Coupled Receptor Bound to Cyclopentanoindole Antagonist, Predicted Using the DuplexBiHelix Modification of the GEnSeMBLE Method. Journal of Chemical Theory and Computation, 2018, 14, 1624-1642.	2.3	13
598	Mechanical softening of thermoelectric semiconductor Mg2Si from nanotwinning. Scripta Materialia, 2018, 157, 90-94.	2.6	13
599	Mechanism and kinetics for both thermal and electrochemical reduction of N ₂ catalysed by Ru(0001) based on quantum mechanics. Physical Chemistry Chemical Physics, 2019, 21, 17605-17612.	1.3	13
600	Effect of Co doping on mechanism and kinetics of ammonia synthesis on Fe(1â€ ⁻ 1â€ ⁻ 1) surface. Journal of Catalysis, 2019, 370, 364-371.	3.1	13
601	DFT Mechanistic Study of Methane Mono-Esterification by Hypervalent Iodine Alkane Oxidation Process. Journal of Physical Chemistry C, 2019, 123, 15674-15684.	1.5	13
602	First-Principles Molecular Dynamics in Metal-Halide Perovskites: Contrasting Generalized Gradient Approximation and Hybrid Functionals. Journal of Physical Chemistry Letters, 2021, 12, 11886-11893.	2.1	13
603	Thermodynamic properties and homogeneous nucleation rates for surfaceâ€melted physical clusters. Journal of Chemical Physics, 1996, 105, 7648-7663.	1.2	12
604	Correlation Analysis of Chemical Bonds (CACB) II:  Quantum Mechanical Operators for Classical Chemical Concepts. Journal of Physical Chemistry A, 2000, 104, 2221-2229.	1.1	12
605	Catalytic role of boron atoms in self-interstitial clustering in Si. Applied Physics Letters, 2003, 83, 1047-1049.	1.5	12
606	Iridium complexes bearing a PNP ligand, favoring facile C(sp3)–H bond cleavage. Dalton Transactions, 2011, 40, 9094.	1.6	12
607	An etÂal. Reply:. Physical Review Letters, 2017, 118, 089602.	2.9	12
608	Mechanical properties of thermoelectric lanthanum telluride from quantum mechanics. Journal Physics D: Applied Physics, 2017, 50, 274002.	1.3	12
609	Predictive simulation of non-steady-state transport of gases through rubbery polymer membranes. Polymer, 2018, 134, 125-142.	1.8	12
610	Analysis of dynamics, stability, and flow fields' structure of an accelerated hydrodynamic discontinuity with interfacial mass flux by a general matrix method. Physics of Plasmas, 2018, 25, .	0.7	12
611	Synergetic Evolution of Sacrificial Bonds and Strain-Induced Defects Facilitating Large Deformation of the Bi ₂ Te ₃ Semiconductor. ACS Applied Energy Materials, 2020, 3, 3042-3048.	2.5	12
612	Predictions of Chemical Shifts for Reactive Intermediates in CO2 Reduction under Operando Conditions. ACS Applied Materials & Interfaces, 2021, 13, 31554-31560.	4.0	12

#	Article	IF	CITATIONS
613	Identification and characterization of an atypical Cαs-biased β ₂ AR agonist that fails to evoke airway smooth muscle cell tachyphylaxis. Proceedings of the National Academy of Sciences of the United States of America, 2021, 118, .	3.3	12
614	Free energy and surface tension of arbitrarily large Mackay icosahedral clusters. Journal of Chemical Physics, 1995, 102, 3322-3330.	1.2	11
615	Thermal Decomposition of Energetic Materials by ReaxFF Reactive Molecular Dynamics. AIP Conference Proceedings, 2006, , .	0.3	11
616	Methane Activation with Rhenium Catalysts. 1. Bidentate Oxygenated Ligands. Organometallics, 2007, 26, 1505-1511.	1.1	11
617	Electron Transport through Cyclic Disulfide Molecular Junctions with Two Different Adsorption States at the Contact: A Density Functional Theory Study. Journal of Physical Chemistry C, 2008, 112, 8715-8720.	1.5	11
618	Reactive molecular dynamics force field for the dissociation of light hydrocarbons on Ni(111). Molecular Simulation, 2008, 34, 967-972.	0.9	11
619	Nucleation of Graphene Layers on Magnetic Oxides: Co ₃ O ₄ (111) and Cr ₂ O ₃ (0001) from Theory and Experiment. Journal of Physical Chemistry Letters, 2017, 8, 188-192.	2.1	11
620	The Transition Metal Catalyzed [Ï€2s + Ï€2s + Ïf2s + Ïf2s] Pericyclic Reaction: Woodward–Hoffmann Rules, Aromaticity, and Electron Flow. Journal of the American Chemical Society, 2020, 142, 19033-19039.	6.6	11
621	Spatiotemporal Temperature and Pressure in Thermoplasmonic Gold Nanosphere–Water Systems. ACS Nano, 2021, 15, 6276-6288.	7.3	11
622	Interfacial Interactions in a Model Composite Material: Insights into α → β Phase Transition of the Magnetite Reinforced Poly(Vinylidene Fluoride) Systems by All-Atom Molecular Dynamics Simulation. Journal of Physical Chemistry C, 2021, 125, 21635-21644.	1.5	11
623	Controlling the Shapes of Nanoparticles by Dopant-Induced Enhancement of Chemisorption and Catalytic Activity: Application to Fe-Based Ammonia Synthesis. ACS Nano, 2021, 15, 1675-1684.	7.3	11
624	Addressing amorphization and transgranular fracture of B ₄ C through Si doping and TiB ₂ microparticle reinforcing. Journal of the American Ceramic Society, 2022, 105, 2959-2977.	1.9	11
625	The symmetric group and the spin generalized scf method. International Journal of Quantum Chemistry, 1969, 4, 593-600.	1.0	10
626	First principles-based multiparadigm, multiscale strategy for simulating complex materials processes with applications to amorphous SiC films. Journal of Chemical Physics, 2015, 142, 174703.	1.2	10
627	Room-Temperature Lithium Phases from Density Functional Theory. Journal of Physical Chemistry C, 2016, 120, 27104-27108.	1.5	10
628	Computational Design of a Pincer Phosphinito Vanadium ((OPO)V) Propane Monoxygenation Homogeneous Catalyst Based on the Reduction-Coupled Oxo Activation (ROA) Mechanism. ACS Catalysis, 2017, 7, 356-364.	5.5	10
629	Theoretical pulse charge for the optimal inhibition of growing dendrites. MRS Advances, 2018, 3, 1201-1207.	0.5	10
630	Grain Boundaries Softening Thermoelectric Oxide BiCuSeO. ACS Applied Materials & Interfaces, 2018, 10, 6772-6777.	4.0	10

#	Article	IF	CITATIONS
631	Determining ideal strength and failure mechanism of thermoelectric CulnTe2 through quantum mechanics. Journal of Materials Chemistry A, 2018, 6, 11743-11750.	5.2	10
632	Reply to the â€~Comment on "The chemical reactions in electrosprays of water do not always correspond to those at the pristine air–water interfaceâ€ê€™ by A. J. Colussi and S. Enami, <i>Chem. Sci.</i> , 2019, 10 , DOI: 10.1039/c9sc00991d. Chemical Science, 2019, 10, 8256-8261.	3.7	10
633	Inertial dynamics of an interface with interfacial mass flux: Stability and flow fields' structure, inertial stabilization mechanism, degeneracy of Landau's solution, effect of energy fluctuations, and chemistry-induced instabilities. Physics of Fluids, 2020, 32, 082105.	1.6	10
634	Enhancing the Detonation Properties of Liquid Nitromethane by Adding Nitro-Rich Molecule Nitryl Cyanide. Journal of Physical Chemistry C, 2020, 124, 9787-9794.	1.5	10
635	Diverse Phases of Carbonaceous Materials from Stochastic Simulations. ACS Nano, 2021, 15, 6369-6385.	7.3	10
636	Models for the behavior of boron carbide in extreme dynamic environments. Journal of the American Ceramic Society, 2022, 105, 3043-3061.	1.9	10
637	Nanotwin-induced ductile mechanism in thermoelectric semiconductor PbTe. Matter, 2022, 5, 1839-1852.	5.0	10
638	Shouldering in B diffusion profiles in Si: Role of di-boron diffusion. Applied Physics Letters, 2003, 83, 3501-3503.	1.5	9
639	Initial Chemical Events in the Energetic Material RDX under Shock Loading: Role of Defects. AIP Conference Proceedings, 2004, , .	0.3	9
640	Possible performance improvement in [2]catenane molecular electronic switches. Applied Physics Letters, 2006, 88, 163112.	1.5	9
641	Selectivity and specificity of substrate binding in methionyl-tRNA synthetase. Protein Science, 2009, 13, 2693-2705.	3.1	9
642	The para-substituent effect and pH-dependence of the organometallic Baeyer–Villiger oxidation of rhenium–carbon bonds. Dalton Transactions, 2012, 41, 3758.	1.6	9
643	Deformation Induced Solid–Solid Phase Transitions in Gamma Boron. Chemistry of Materials, 2014, 26, 4289-4298.	3.2	9
644	Quantum Mechanical and Experimental Validation that Cyclobis(paraquatâ€≺i>pâ€phenylene) Forms a 1:1 Inclusion Complex with Tetrathiafulvalene. Chemistry - A European Journal, 2016, 22, 2736-2745.	1.7	9
645	Polarizable Charge Equilibration Model for Transition-Metal Elements. Journal of Physical Chemistry A, 2018, 122, 9350-9358.	1.1	9
646	Free Energy Landscape of Sodium Solvation into Graphite. Journal of Physical Chemistry C, 2018, 122, 20064-20072.	1.5	9
647	Li-diffusion at the interface between Li-metal and [Pyr14][TFSI]-ionic liquid: <i>Ab initio</i> molecular dynamics simulations. Journal of Chemical Physics, 2020, 152, 031101.	1.2	9
648	Morphometry of Dendritic Materials in Rechargeable Batteries. Journal of Power Sources, 2021, 481, 228914.	4.0	9

#	ARTICLE	IF	CITATIONS
649	Mechanistic Studies of Styrene Production from Benzene and Ethylene Using [(Î- ² -C ₂ H ₄) ₂ Rh(Î ¹ /4-OAc)] ₂ as Catalyst Precursor: Identification of a Bis-Rh ^I Mono-Cu ^{II} Complex As the Catalyst. ACS Catalysis, 2021, 11, 5688-5702.	5.5	9
650	Dramatic Change in the Step Edges of the Cu(100) Electrocatalyst upon Exposure to CO: <i>Operando</i> Observations by Electrochemical STM and Explanation Using Quantum Mechanical Calculations. ACS Catalysis, 2021, 11, 12068-12074.	5.5	9
651	Increasing Oxygen Balance Leads to Enhanced Performance in Environmentally Acceptable High-Energy Density Materials: Predictions from First-Principles Molecular Dynamics Simulations. ACS Applied Materials & Interfaces, 2022, 14, 5257-5264.	4.0	9
652	Programmable siRNA pro-drugs that activate RNAi activity in response to specific cellular RNA biomarkers. Molecular Therapy - Nucleic Acids, 2022, 27, 797-809.	2.3	9
653	Manganese Catalyzed Partial Oxidation of Light Alkanes. ACS Catalysis, 2022, 12, 5356-5370.	5.5	9
654	Si + SiH4 Reactions and Implications for Hot-Wire CVD of a-Si:H: Computational Studies. Materials Research Society Symposia Proceedings, 2000, 609, 611.	0.1	8
655	Ordering and dimensional crossovers in metallic glasses and liquids. Physical Review B, 2017, 95, .	1.1	8
656	Reaction mechanisms and sensitivity of silicon nitrocarbamate and related systems from quantum mechanics reaction dynamics. Journal of Materials Chemistry A, 2018, 6, 5082-5097.	5.2	8
657	Permeation of CO ₂ and N ₂ through glassy poly(dimethyl phenylene) oxide under steady―and presteadyâ€state conditions. Journal of Polymer Science, 2020, 58, 1207-1228.	2.0	8
658	Hedgehog proteins create a dynamic cholesterol interface. PLoS ONE, 2021, 16, e0246814.	1.1	8
659	The first order L-G phase transition in liquid Ag and Ag-Cu alloys is driven by deviatoric strain. Scripta Materialia, 2021, 194, 113695.	2.6	8
660	Synergic Effects in the Activation of the Sweet Receptor GPCR Heterodimer for Various Sweeteners Predicted Using Molecular Metadynamics Simulations. Journal of Agricultural and Food Chemistry, 2021, 69, 12250-12261.	2.4	8
661	Immobilization of "Capping Arene―Cobalt(II) Complexes on Ordered Mesoporous Carbon for Electrocatalytic Water Oxidation. ACS Catalysis, 2021, 11, 15068-15082.	5.5	8
662	Manager–worker-based model for the parallelization of quantum Monte Carlo on heterogeneous and homogeneous networks. Journal of Computational Chemistry, 2008, 29, 8-16.	1.5	7
663	The quantum mechanics derived atomistic mechanism underlying the acceleration of catalytic CO oxidation on Pt(110) by surface acoustic waves. Journal of Materials Chemistry A, 2016, 4, 12036-12045.	5.2	7
664	The mechanism for catalytic hydrosilylation by bis(imino)pyridine iron olefin complexes supported by broken symmetry density functional theory. Dalton Transactions, 2017, 46, 12507-12515.	1.6	7
665	First principles-based multiscale atomistic methods for input into first principles nonequilibrium transport across interfaces. Proceedings of the National Academy of Sciences of the United States of America, 2019, 116, 18193-18201.	3.3	7
666	Anomalies in Supercooled Water at â^¼230 K Arise from a 1D Polymer to 2D Network Topological Transformation. Journal of Physical Chemistry Letters, 2019, 10, 6267-6273.	2.1	7

#	Article	IF	CITATIONS
667	Predicted structure of fully activated human bitter taste receptor TAS2R4 complexed with G protein and agonists. QRB Discovery, 2021, 2, .	0.6	7
668	The G protein-first activation mechanism of opioid receptors by Gi protein and agonists. QRB Discovery, 2021, 2, .	0.6	7
669	Noncovalent Immobilization of Pentamethylcyclopentadienyl Iridium Complexes on Ordered Mesoporous Carbon for Electrocatalytic Water Oxidation. Small Science, 2021, 1, 2100037.	5.8	7
670	Temperature-dependent anharmonic effects on shear deformability of Bi2Te3 semiconductor. Scripta Materialia, 2021, 202, 114016.	2.6	7
671	In-Silico Screening the Nitrogen Reduction Reaction on Single-Atom Electrocatalysts Anchored on MoS2. Topics in Catalysis, 2022, 65, 234-241.	1.3	7
672	An optimized initialization algorithm to ensure accuracy in quantum Monte Carlo calculations. Journal of Computational Chemistry, 2008, 29, 2335-2343.	1.5	6
673	Surface and Electronic Properties of Hydrogen Terminated Si [001] Nanowires. Journal of Physical Chemistry C, 2011, 115, 12586-12591.	1.5	6
674	Predicted Ligands for the Human Urotensinâ€I G Protein oupled Receptor with Some Experimental Validation. ChemMedChem, 2014, 9, 1732-1743.	1.6	6
675	Stability of NNO and NPO Nanotube Crystals. Journal of Physical Chemistry Letters, 2014, 5, 485-489.	2.1	6
676	The Predicted Ensemble of Lowâ€Energy Conformations of Human Somatostatin Receptor Subtypeâ€5 and the Binding of Antagonists. ChemMedChem, 2015, 10, 650-661.	1.6	6
677	Shift-Collapse Acceleration of Generalized Polarizable Reactive Molecular Dynamics for Machine Learning-Assisted Computational Synthesis of Layered Materials. , 2018, , .		6
678	In Silico Optimization of Organic–Inorganic Hybrid Perovskites for Photocatalytic Hydrogen Evolution Reaction in Acidic Solution. Journal of Physical Chemistry C, 2018, 122, 20918-20922.	1.5	6
679	The PX Motif of DNA Binds Specifically to <i>Escherichia coli</i> DNA Polymerase I. Biochemistry, 2019, 58, 575-581.	1.2	6
680	Toward Concurrent Engineering of the M1-Based Catalytic Systems for Oxidative Dehydrogenation (ODH) of Alkanes. Topics in Catalysis, 2020, 63, 1667-1681.	1.3	6
681	Discovery of Dramatically Improved Ammonia Synthesis Catalysts through Hierarchical High-Throughput Catalyst Screening of the Fe(211) Surface. Chemistry of Materials, 2020, 32, 9914-9924.	3.2	6
682	Pulse Reverse Protocol for efficient suppression of dendritic micro-structures in rechargeable batteries. Electrochimica Acta, 2021, 367, 137469.	2.6	6
683	Design of robust 2,2′-bipyridine ligand linkers for the stable immobilization of molecular catalysts on silicon(111) surfaces. Physical Chemistry Chemical Physics, 2021, 23, 9921-9929.	1.3	6
684	Reduction of N ₂ to Ammonia by Phosphate Molten Salt and Li Electrode: Proof of Concept Using Quantum Mechanics. Journal of Physical Chemistry Letters, 2021, 12, 1696-1701.	2.1	6

#	Article	IF	CITATIONS
685	Operando Electrochemical Spectroscopy for CO on Cu(100) at pH 1 to 13: Validation of Grand Canonical Potential Predictions. ACS Catalysis, 2021, 11, 3173-3181.	5.5	6
686	Understanding Reaction Networks through Controlled Approach to Equilibrium Experiments Using Transient Methods. Journal of the American Chemical Society, 2021, 143, 10998-11006.	6.6	6
687	Predicted Structure of Fully Activated Tas1R3/1R3′ Homodimer Bound to G Protein and Natural Sugars: Structural Insights into G Protein Activation by a Class C Sweet Taste Homodimer with Natural Sugars. Journal of the American Chemical Society, 2021, 143, 16824-16838.	6.6	6
688	Biased β-Agonists Favoring Gs over β-Arrestin for Individualized Treatment of Obstructive Lung Disease. Journal of Personalized Medicine, 2022, 12, 331.	1.1	6
689	Room temperature negative differential resistance of a monolayer molecular rotor device. Applied Physics Letters, 2009, 95, 093503.	1.5	5
690	Multiscale modeling of interaction of alane clusters on Al(111) surfaces: A reactive force field and infrared absorption spectroscopy approach. Journal of Chemical Physics, 2010, 132, 084509.	1.2	5
691	CCl Radicals As a Carbon Source for Diamond Thin Film Deposition. Journal of Physical Chemistry Letters, 2014, 5, 481-484.	2.1	5
692	Reaction Mechanism for Ammonia Activation in the Selective Ammoxidation of Propene on Bismuth Molybdates. Journal of Physical Chemistry C, 2015, 119, 27370-27381.	1.5	5
693	Elucidating challenges of reactions with correlated reactant and product binding energies on an example of oxygen reduction reaction. Journal of Molecular Catalysis A, 2016, 423, 449-456.	4.8	5
694	Homology modeling and molecular docking studies of Drosophila and Aedes sex peptide receptors. Journal of Molecular Graphics and Modelling, 2016, 66, 115-122.	1.3	5
695	Discovery of Novel Biased Opioid Receptor Ligands through Structureâ€Based Pharmacophore Virtual Screening and Experiment. ChemMedChem, 2019, 14, 1783-1794.	1.6	5
696	Scalable Reactive Molecular Dynamics Simulations for Computational Synthesis. Computing in Science and Engineering, 2019, 21, 64-75.	1.2	5
697	Intrinsic mechanical behavior of MgAgSb thermoelectric material: An ab initio study. Journal of Materiomics, 2020, 6, 24-32.	2.8	5
698	Comparing the oxygen reduction reaction on selectively edge halogen doped graphene from quantum mechanics. Journal of Catalysis, 2020, 381, 295-307.	3.1	5
699	Real-time control of dendritic propagation in rechargeable batteries using adaptive pulse relaxation. Journal of Chemical Physics, 2021, 154, 194702.	1.2	5
700	Entropic Stabilization of Water at Graphitic Interfaces. Journal of Physical Chemistry Letters, 2021, 12, 9162-9168.	2.1	5
701	Structures and Agonist Binding Sites of Bitter Taste Receptor TAS2R5 Complexed with Gi Protein and Validated against Experiment. Journal of Physical Chemistry Letters, 2021, 12, 9293-9300.	2.1	5
702	Effective Hamiltonians for motions with disparate time scales: The quantum shell model and the classical statistical shell model. Journal of Chemical Physics, 1993, 98, 1451-1457.	1.2	4

#	Article	IF	CITATIONS
703	Pressure Induced Phase Transformations in Silica. Materials Research Society Symposia Proceedings, 1997, 492, 287.	0.1	4
704	Formation of water at a Pt(111) surface: A study using the reactive force field (ReaxFF). Materials Research Society Symposia Proceedings, 2005, 900, 1.	0.1	4
705	Molecular Modeling of Carbohydrates with No Charges, No Hydrogen Bonds, and No Atoms. ACS Symposium Series, 2006, , 271-284.	0.5	4
706	Recent Advances in Selective Oxidation Catalysis. Topics in Catalysis, 2008, 50, 1-1.	1.3	4
707	Computational Prediction and Biochemical Analyses of New Inverse Agonists for the CB1 Receptor. Journal of Chemical Information and Modeling, 2016, 56, 201-212.	2.5	4
708	Asymmetric twins in boron rich boron carbide. Physical Chemistry Chemical Physics, 2018, 20, 13340-13347.	1.3	4
709	A coarse-grain force field based on quantum mechanics (CGq FF) for molecular dynamics simulation of poly(ethylene glycol)- <i>block</i> -poly(ε-caprolactone) (PEG- <i>b</i> -PCL) micelles. Physical Chemistry Chemical Physics, 2020, 22, 24028-24040.	1.3	4
710	Group Vibrational Mode Assignments as a Broadly Applicable Tool for Characterizing Ionomer Membrane Structure as a Function of Degree of Hydration. Chemistry of Materials, 2020, 32, 1828-1843.	3.2	4
711	A Novel Method for Estimating the Charge Equilibrium within the Dendrites of Rechargeable Batteries. Computational Materials Science, 2021, 187, 110059.	1.4	4
712	Rhodium and Iridium Complexes Bearing "Capping Arene―Ligands: Synthesis and Characterization. Organometallics, 2021, 40, 2808-2825.	1.1	4
713	Identifying the Imperative Role of Metal–Olefin Interactions in Catalytic C–O Reductive Elimination from Nickel(II). ACS Catalysis, 2021, 11, 10208-10222.	5.5	4
714	Compression Induced Deformation Twinning Evolution in Liquid-Like Cu ₂ Se. ACS Applied Materials & Interfaces, 2022, 14, 18671-18681.	4.0	4
715	Reaction Mechanism Underlying Pd(II)-Catalyzed Oxidative Coupling of Ethylene and Benzene to Form Styrene: Identification of a Cyclic Mono-Pd ^{II} Bis-Cu ^{II} Complex as the Active Catalyst. Organometallics, 0, , .	1.1	4
716	Parallel Calculation of Electron-Transfer and Resonance Matrix Elements of Hartree—Fock and Generalized Valence Bond Wave Functions. ACS Symposium Series, 1995, , 84-96.	0.5	3
717	The optimum orbitals for the H2 + D⇋H + HD exchange reaction. International Journal of Quantum Chemistry, 1969, 3, 63-66.	1.0	3
718	Identifying multiple active conformations in the G protein-coupled receptor activation landscape using computational methods. Methods in Cell Biology, 2017, 142, 173-186.	0.5	3
719	Bulk Properties of Amorphous Lithium Dendrites. ECS Transactions, 2017, 80, 365-370.	0.3	3
720	The Mechanism of Deformation and Failure of In4Se3 Based Thermoelectric Materials. ACS Applied Energy Materials, 2020, 3, 1054-1062.	2.5	3

#	Article	IF	CITATIONS
721	Coarse-grained force-field for large scale molecular dynamics simulations of polyacrylamide and polyacrylamide-gels based on quantum mechanics. Physical Chemistry Chemical Physics, 2021, 23, 10909-10918.	1.3	3
722	Selfâ€assembly mechanism of PEGâ€ <i>b</i> â€PCL and PEGâ€ <i>b</i> â€PBOâ€ <i>b</i> â€PCL amphiphilic copoly micelles in aqueous solution from coarse grain modeling. Journal of Polymer Science, 2021, 59, 614-626.	ymer 2.0	3
723	Functionalization of RhIII–Me Bonds: Use of "Capping Arene―Ligands to Facilitate Me–X Reductive Elimination. Organometallics, 2021, 40, 1889-1906.	1.1	3
724	Transport properties of imidazolium based ionic liquid electrolytes from molecular dynamics simulations. Electrochemical Science Advances, 0, , e2100007.	1.2	3
725	Doubleâ€Exchangeâ€Induced in situ Conductivity in Nickelâ€Based Oxyhydroxides: An Effective Descriptor for Electrocatalytic Oxygen Evolution. Angewandte Chemie, 2021, 133, 16584-16592.	1.6	3
726	Strengthening boron carbide by doping Si into grain boundaries. Journal of the American Ceramic Society, 2022, 105, 2978-2989.	1.9	3
727	Development of the ReaxFF Reactive Force Field for Cu/Si Systems with Application to Copper Cluster Formation during Cu Diffusion Inside Silicon. Journal of Physical Chemistry C, 2021, 125, 19455-19466.	1.5	3
728	Structure, Energetics, and Spectra for the Oxygen Vacancy in Rutile: Prominence of the Ti–H _O –Ti Bond. Journal of Physical Chemistry Letters, 2021, 12, 10175-10181.	2.1	3
729	Reaction Mechanism and Energetics of Decomposition of Tetrakis(1,3-dimethyltetrazol-5-imidoperchloratomanganese(II)) from Quantum-Mechanics-based Reactive Dynamics. Journal of the American Chemical Society, 2021, 143, 16960-16975.	6.6	3
730	Order-Tuned Deformability of Bismuth Telluride Semiconductors: An Energy-Dissipation Strategy for Large Fracture Strain. ACS Applied Materials & Interfaces, 2021, 13, 57629-57637.	4.0	3
731	Complete inhibition of a polyol nucleation by a micromolar biopolymer additive. Cell Reports Physical Science, 2022, 3, 100723.	2.8	3
732	Summary Abstract: Mott insulator model of the Si(111)â€(2×1) surface. Journal of Vacuum Science and Technology, 1982, 21, 328-329.	1.9	2
733	Recent Advances in Simulation of Dendritic Polymers. Materials Research Society Symposia Proceedings, 1998, 543, 299.	0.1	2
734	Molecular Dynamics Simulations of Supercooled Liquid Metals and Glasses. Materials Research Society Symposia Proceedings, 2000, 644, 231.	0.1	2
735	Reply to Head-Gordon and Paesani: Liquid water, a branched polymer with â^1⁄4100-fs short-lived heterogeneous hydrogen bonds. Proceedings of the National Academy of Sciences of the United States of America, 2019, 116, 20257-20258.	3.3	2
736	London Dispersion Corrections to Density Functional Theory for Transition Metals Based on Fitting to Experimental Temperature-Programmed Desorption of Benzene Monolayers. Journal of Physical Chemistry Letters, 2021, 12, 73-79.	2.1	2
737	The L–G phase transition in binary Cu–Zr metallic liquids. Physical Chemistry Chemical Physics, 2021, 24, 497-506.	1.3	2
738	Experimental and Theoretical Comparison of Potential-dependent Methylation on Chemically Exfoliated WS ₂ and MoS ₂ . ACS Applied Materials & Interfaces, 2022, 14, 9744-9753.	4.0	2

#	Article	IF	CITATIONS
739	Selective Signal Capture from Multidimensional GPCR Outputs with Biased Agonists: Progress Towards Novel Drug Development. Molecular Diagnosis and Therapy, 2022, 26, 383-396.	1.6	2
740	Effects of Catalyst Promoters on the Growth of Single-Layer Carbon Nanotubes. Materials Research Society Symposia Proceedings, 1994, 359, 69.	0.1	1
741	Deformation Behavior of FCC Crystalline Metallic Nanowires Under High Strain Rates. Materials Research Society Symposia Proceedings, 1998, 554, 367.	0.1	1
742	Reactive Molecular Dynamics of Shock- and Shear-Induced Chemistry in Energetic Materials for Future Force Insensitive Munitions. , 2009, , .		1
743	Direct growth of graphene on dielectric substrates: Epitaxy at incommensurate and reactive interfaces. , 2016, , .		1
744	Ordered three-fold symmetric graphene oxide/buckled graphene/graphene heterostructures on MgO(111) by carbon molecular beam epitaxy. Journal of Materials Chemistry C, 2018, 6, 4225-4233.	2.7	1
745	Design of a One-Dimensional Stacked Spin Peierls System with Room-Temperature Switching from Quantum Mechanical Predictions. Journal of Physical Chemistry Letters, 2019, 10, 6432-6437.	2.1	1
746	New Quantum Mechanics Based Methods for Multiscale Simulations with Applications to Reaction Mechanisms for Electrocatalysis. Topics in Catalysis, 2020, 63, 1658-1666.	1.3	1
747	Structural failure of layered thermoelectric In4Se3-δ semiconductors is dominated by shear slippage. Acta Materialia, 2020, 187, 84-90.	3.8	1
748	<i>Response</i> : Magnon-Exchange Pairing and Superconductivity. Science, 1989, 243, 547-548.	6.0	1
749	Electrochemical Performance and Structures of Chromium and Molybdenum-Doped Îμ-Li _{<i>x</i>} VOPO ₄ Predicted as Promising Cathodes for Next Generation Lithium-Ion Batteries. Journal of Physical Chemistry C, 2021, 125, 275-282.	1.5	1
750	Deformation and Failure Mechanisms of Thermoelectric Type-I Clathrate Ba ₈ Au ₆ Ge ₄₀ . ACS Applied Materials & Interfaces, 2022, 14, 4326-4334.	4.0	1
751	Vibrational Spectroscopy Signatures of Catalytically Relevant Configurations for N ₂ Reduction to NH ₃ on Fe Surfaces via Density Functional Theory. Journal of Physical Chemistry C, 2021, 125, 27919-27930.	1.5	1
752	Shear Banding in Binary Cu-Zr Metallic Glass: Comparison of the G-Phase With L-Phase. Frontiers in Materials, 2022, 9, .	1.2	1
753	Valence Bond Charge Transfer Theory for Predicting Nonlinear Optical Properties of Organic Materials. ACS Symposium Series, 1995, , 341-358.	0.5	Ο
754	Diamond and Polycrystalline Diamond for MEMS Applications: Simulations and Experiments. Materials Research Society Symposia Proceedings, 1998, 546, 109.	0.1	0
755	Structural and Dynamic Properties of Hexadecane Lubricants under Shear Flow in a Confined Geometry. ACS Symposium Series, 2001, , 158-177.	0.5	0
756	First-principles study of charge transport across alkene thiolate self-assembled monolayers. , 2006, , .		0

#	Article	IF	CITATIONS
757	PREDICTION OF STRUCTURE OF G-PROTEIN COUPLED RECEPTORS AND OF BOUND LIGANDS, WITH APPLICATIONS FOR DRUG DESIGN. , 2007, , .		0
758	A nano-scale molecular rotor device for high density memory application. , 2009, , .		0
759	Lithium Dendrite Inhibition on Post-Charge Anode Surface: The Kinetics Role. Materials Research Society Symposia Proceedings, 2015, 1774, 31-39.	0.1	0
760	Preface to "Advances in Heterogeneous Catalysis and Electrocatalysis Including New Insights from Surface Science and Quantum Mechanics, Published in Honor of Professor Robert K. Grasselli, Irsee VIII Symposium Kloster Irsee, Germany 23–26 May 2019 (Irsee VIII)― Topics in Catalysis, 2020, 63, 1645-1646.	1.3	0
761	Quantum mechanics based mechanisms for selective activation of hydrocarbons by mixed metal oxide heterogeneous catalysts – A tribute to Robert Grasselli. Catalysis Today, 2021, 363, 3-9.	2.2	0
762	Structural basis of human cannabinoid CB1 G protein oupled receptor activation. FASEB Journal, 2013, 27, .	0.2	0
763	Extracellular interaction between Neurotrophic factorâ€Î±1 and HTR1E serotonin receptor promotes cell survival. FASEB Journal, 2020, 34, 1-1.	0.2	0
764	5HTR1E receptor interacts with Neurotrophic factorâ€Î±1 and serotonin to activate two distinct signaling pathways. FASEB Journal, 2022, 36, .	0.2	0
765	Unraveling the capacitive effect in the vacancy-heterostructure WTe2/MoTe2 for hydrogen evolution reaction by the grand canonical potential kinetics. International Journal of Hydrogen Energy, 2022, , .	3.8	0